
Article:
Gonzalez-Delgado, L.S., Walters-Morgan, H., Salamaga, B. et al. (7 more authors) (2019) Two-site recognition of Staphylococcus aureus peptidoglycan by lysostaphin SH3b. Nature Chemical Biology. ISSN 1552-4450

https://doi.org/10.1038/s41589-019-0393-4

Two site recognition of *Staphylococcus aureus* peptidoglycan by lysostaphin SH3b

Luz S. Gonzalez-Delgado[1,2†], Hannah Waters-Morgan[3†], Bartłomiej Salamaga[1,2], Angus J Robertson[1,2], Andrea M. Hounslow[1,2], Elżbieta Jagielska[4], Izabela Sabala[4], Mike P. Williamson[1,2]*, Andrew L. Lovering[3]* and Stéphane Mesnage[1,2]*

[1] Department of Molecular Biology and Biotechnology, University of Sheffield, Firth Court, Western Bank, Sheffield, UK;

[2] Krebs Institute, University of Sheffield, Firth Court, Western Bank, Sheffield, UK;

[3] Institute of Microbiology and Infection & School of Biosciences, University of Birmingham, Birmingham, UK

[4] International Institute of Molecular and Cell Biology, Warsaw, Poland

[†] These authors contributed equally to this work

* Corresponding authors

Email: s.mesnage@sheffield.ac.uk; m.williamson@sheffield.ac.uk; a.lovering@bham.ac.uk

Short title: Peptidoglycan recognition by lysostaphin

Abstract (150 words)

Lysostaphin is a bacteriolytic enzyme targeting peptidoglycan, the essential component of the bacterial cell envelope. It displays a very potent and specific activity towards staphylococci, including methicillin-resistant *Staphylococcus aureus* (MRSA). Lysostaphin causes rapid cell lysis and disrupts biofilms, and is therefore a therapeutic agent of choice to eradicate staphylococcal infections. The C-terminal SH3b domain of lysostaphin recognizes peptidoglycans containing a pentaglycine crossbridge and has been proposed to drive the preferential digestion of staphylococcal cell walls. Here, we elucidate the molecular mechanism underpinning recognition of staphylococcal peptidoglycan by the lysostaphin SH3b domain. We show that the pentaglycine crossbridge and the peptide stem are recognized by two independent binding sites located on opposite sides of the SH3b domain, thereby inducing a clustering of SH3b domains. We propose that this unusual binding mechanism allows a synergistic and structurally dynamic recognition of *S. aureus* peptidoglycan and underpins the potent bacteriolytic activity of this enzyme.

Introduction

Lysostaphin is a bacteriolytic enzyme produced and secreted by *Staphylococcus simulans* biovar *staphylolyticus* [1]. This exotoxin has a potent activity against a wide range of staphylococci including the opportunistic nosocomial pathogen *Staphylococcus aureus* [2]. It displays endopeptidase activity and cleaves the pentaglycine crossbridges present in the essential component of the bacterial cell wall (peptidoglycan), leading to rapid cell lysis. In *S. simulans* biovar *staphylolyticus,* immunity to lysostaphin is conferred by Lif, an aminoacyl transferase that introduces serine residues into peptidoglycan crossbridges [3]. This modification dramatically reduces susceptibility to lysostaphin.

Due to its powerful antistaphylococcal activity against both planktonic cells and biofilms [4], lysostaphin has been extensively studied as a therapeutic agent to treat infections caused by methicillin resistant *S. aureus* (MRSA) [5-11]. Recent studies have reported the design of lysostaphin variants with a reduced antigenicity and enhanced therapeutic efficacy [12,13] as well as strategies to harness the bactericidal activity of this toxin [14-16]. Collectively, the studies published have demonstrated that lysostaphin represents a credible therapeutic agent to combat staphylococcal infections, either alone or in combination with antibiotics [17].

Lysostaphin is a modular hydrolase produced as a pre-proenzyme. It comprises a signal peptide, 15 N-terminal repeats of 13 amino acids, a catalytic domain with glycylglycyl endopeptidase activity and a C-terminal peptidoglycan binding domain of 92 residues [3]. The specificity of lysostaphin towards staphylococci has been attributed to its binding domain, which recognizes pentaglycine crossbridges [18,19]. Recent crystallographic studies have confirmed early models and showed that the pentaglycine stem is recognized by a shallow groove formed between strands β1-β2 and the RT loop, the binding specificity being essentially conferred by steric hindrance [20]. Despite this exquisite recognition mechanism, the SH3b domain displays a very weak affinity for the pentaglycine stems and binding has been shown to be optimal with multimeric peptidoglycan fragments, suggesting a mechanism more complex than initially anticipated [20,21].

Here, we combine NMR and X-ray crystallography to elucidate the mechanism underpinning the recognition of staphylococcal peptidoglycans by the lysostaphin SH3b domain. We show that the SH3b domain contains two binding sites located on opposite sides of the protein, allowing a mutually exclusive recognition of these two peptidoglycan moieties. The recognition of the pentaglycine crossbridge and the peptide stem is therefore shared by two independent SH3b domains, allowing protein clustering on the peptidoglycan. We propose that

the combination of low affinity and high off-rate binding results in a synergistic and structurally dynamic binding that is particularly suitable for the recognition of non-contiguous epitopes of mature, physiological peptidoglycan. This unusual mechanism underpins the potent activity of lysostaphin and its capacity to punch holes in the cell walls to cause rapid cell lysis.

Results

NMR analysis of SH3b-peptidoglycan interactions

We sought to investigate the mechanism underpinning SH3b-PG interaction using NMR titrations with a panel of ligands of increasing complexity. Six ligands were produced, either by solid-phase synthesis or purified from *S. aureus* PG following digestion by hydrolytic enzymes (Supplementary Fig. 1). The ligands tested corresponded to a tetrasaccharide (GlcNAc-MurNAc- GlcNAc-MurNAc; GMGM), a pentaglycine crossbridge (GGGGG; G5), a tetrapeptide stem (AγQKA; P4), a tetrapeptide with the pentaglycine as a lateral chain (AγQK[GGGGG]A; P4-G5), a disaccharide-peptide dimer (GlcNAc-MurNAc-AγQK[GGGGG]AA- GlcNAc-MurNAc-AγQK[GGGGG]A; $(GM\text{-}P4\text{-}G5)_2$) and the peptide AγQK[GGGGG]AA-AγQKA (P5-G5-P4) containing two peptide stems crosslinked via a single pentaglycine crossbridge.

Complete resonance assignment of the doubly labelled SH3b domain was obtained using standard triple resonance experiments (Supplementary Fig. 2).The six ligands were used to measure chemical shift perturbations (CSPs) associated with main-chain and side-chain amides (Supplementary Fig. 3 and Supplementary Table 1).

In agreement with previous studies, our results showed that pentaglycine (G5) peptides interact with several residues located in a narrow cleft corresponding to the binding groove originally proposed for *Staphylococcus capitis* ALE-1, a close homolog of Lss. These included residues N405 to Y411, T429, G430, M453, D456 and Y472 (Fig. 1a, Supplementary Fig. 3a). CSPs of the signals corresponding to SH3b residues following addition of this ligand indicated a fast exchange rate with a weak binding affinity in the millimolar range (K_D=890 ± 160μM).

S. aureus peptidoglycan is highly crosslinked and therefore contains mostly tetrapeptide stems (P4). The SH3b domain bound to P4 peptides with a fast exchange rate and a low affinity (K_D=963 ± 198μM), suggesting that this minimal ligand (like the G5 peptide) is not the complete PG motif recognised by the SH3b domain. Surprisingly, residues presenting pronounced chemical shifts upon binding to the P4 ligand were located on the side of the protein opposite to the G5 binding cleft (*e.g.*, N421, I425, A443, V440; Fig. 1b and Supplementary Fig. 3b). Residue R427 side chain also showed a significant CSP. Two hydrophobic residues presenting relatively large CSPs were buried in the structure, suggesting that they were not directly in contact with the P4 ligand (V461 and L473). This observation

implies that whereas binding at G5 is fairly rigid lock-and-key, binding at P4 is more of an induced fit interaction, with adaptation of the protein to fit its ligand.

As expected, a tighter binding was observed for two PG monomer ligands made of the tetrapeptide stem with a pentaglycine lateral chain alone (P4-G5; $K_D = 98 \pm 42$ µM). The most prominent CSPs corresponded to residues previously identified with the simple ligands G5 and P4 in both cases (Fig. 1b,c). Several residues broadened and disappeared with the P4-G5 ligand (N405, I425, V461, G462, Y472 and L473), indicating a slow to medium exchange rate (Supplementary Fig. 3c). Titrations with a synthetic tetrasaccharide $(GlcNAc\text{-}MurNac)_2$ revealed no interactions between the protein and the synthetic disaccharides, suggesting that the sugars do not play a key role in the recognition of peptidoglycan by the SH3b domain.

Next, we studied the binding of SH3b domain to dimeric PG fragments made of two peptide stems crosslinked by a pentaglycine chain. One of these ligands contained a single pentaglycine chain (P5-G5-P4), whilst the other had two (GM-P5-G5-GM-P4-G5). The largest CSPs associated with binding were those previously identified with simpler ligands (G5 and P4) (Fig. 1e,f and Supplementary Fig. 3e,f). The CSPs corresponding to the recognition of the P4/P5 or G5 moieties were typical of a fast exchange rate, with an affinity of 100 ± 34µM for the P5-G5-P4 ligand. In the case of the most complex ligand (GM-P5-G5-GM-P4-G5), we could not determine any binding affinity since the protein started to precipitate in the presence of 4 equivalents of ligand resulting in the disappearance of the signals. One surface residues (W489) located close to residues binding the peptide stem only displayed CSPs with dimeric ligands. Interestingly, the CSPs observed for the larger ligands had fewer large changes than were seen for the simpler ligands (Supplementary Fig. 3).

Collectively, NMR titrations suggested that the SH3b domain recognises both the PG peptide stems and crossbridges via distinct sets of residues located on opposite sides of the protein surface.

Structure of the SH3b-*S. aureus* PG peptide stem complex

We attempted to co-crystallize the SH3b domain with a branched P4-G5 ligand and were successful in obtaining crystals that diffracted to 1.4 Å resolution. Our initial expectation was to observe this ligand binding to the surface of a single SH3b domain but upon solving the structure it was apparent that the G5 was recognized by one domain and P4 by another (symmetry-related copy) as shown in Fig. 2. The 1.4 Å high resolution, synchrotron set is able to trace three of the P4 units (γQKA representing units 2-4) and a lower 2.5 Å home source set

is essentially identical but allows tracing of the full P4 ligand (AγQKA). In our structures, the pentaglycine bridge sits identically to that of other SH3b structures (5LEO), but then projects the crossbridge link (K to G5) and stem peptide (AγQKA) into a pocket located on the opposite side of a second SH3b monomer (Fig. 2a-c). The two SH3 domains make no strong interactions with one another, but display a shape/surface complementarity that allows for close contact around the shared ligand.

The P4 and G5 components of the ligand are at approximately 90˚ angles to one another, and the carbon atoms of the K3 sidechain make favourable contacts with the hydrophobic sidechains of Y407, T422', I424' and W489' (prime used to denote opposing SH3b). Units one to three of the P4 peptidoglycan stem display a linear β-like conformation, with peptide bonds hydrogen-bonding to residues from both SH3b domains: γQ2 NH to carbonyl of K406, K3 NH to carbonyl of D423', and K3 CO to NH of I425'. This arrangement makes for much stronger contacts of the SH3b domains to P3/P4 in comparison to P1/P2, and would place the attached physiological peptidoglycan saccharide units at the edge of both monomers. There is a clearly defined pocket for the terminal D-Ala 4 (Fig. 2d), with the COO- group making a salt-bridge to the sidechain of R427', and a hydrophobic pocket comprised of I424', I425', R433', H458', W460', P474' and W489' surrounding the methyl sidechain of the substrate. Sequence and structure alignments between lysostaphin SH3b (SH3_5) and other proteins indicate that the P4 D-Ala-carboxylate pocket is likely a conserved feature of wider superfamily members (Supplementary Fig. 4), with relevance for both SH3_3 and SH3_4 subgroups. There are no current structures for the latter, but the two SH3_4 domains of *Clostridium* phage lysin phiSM101 each have a carboxylate ligand bound at this position, suggesting an important role for the residues equivalent to lysostaphin R427 [22].

Mutational analysis of the binding activity

We sought to confirm the contribution of the SH3b residues identified by NMR and X-ray crystallography to the recognition of the crossbridge (G5) and peptide stem (P4) ligands. Six single-site substitution mutant domains were produced and analysed by NMR (N405A, M453A, Y472S, I425A, R427M, W489L). ^{15}N HSQC spectra of all mutant domains revealed that these were properly folded, allowing us to measure CSP values in the presence of the maximum concentration of ligand previously used (32 equivalents). As expected, all mutations were associated with a reduction in CSPs when compared to the wild-type domain (Supplementary Fig. 5). We characterised the reduction in binding affinity using a figure of

residual binding, which is defined as the ratio of chemical shift changes of mutant to WT, averaged over all amino acids. Given the weak binding affinities, and the fact that the protein concentration is always lower than the affinity, these correspond roughly to the expected reduction in affinity. Domains with mutations in the residues involved in the interaction with G5 still retained a relatively high residual binding, the N405A mutation having the most pronounced effect (16% residual binding for the N405A mutant, 55.5% for M453A and 24.6% for Y472S). Whilst the I425 still displayed 29.4% residual binding, the mutations R427M and W489L had a major impact on binding to the P4 ligand (1.6% and 6.6% residual binding, respectively). These results confirmed the contribution of the residues identified by NMR and crystallography to the binding of minimal ligands. The limited impact of most of the mutations studied on binding is in agreement with the X-ray and NMR results which revealed that the recognition of peptidoglycan fragments by SH3b domains relies on a complex network of interactions.

Binding of SH3b derivatives to purified PG sacculi

Due to the labour-intensive nature of NMR analyses and the fact that these analyses are limited to study interactions with soluble substrates, we designed a quantitative *in vitro* binding assay with peptidoglycan sacculi which represent the natural substrate of lysostaphin. The SH3b domain was fused to the monomeric fluorescent protein mNeonGreen [23] to follow binding in the presence of increasing amount of peptidoglycan (Fig. 3 and Supplementary Table 2). Recombinant proteins were purified using two chromatography steps including metal affinity and gel filtration. As a first step we measured the binding of SH3b-mNeonGreen fusions to peptidoglycan purified from the WT, *femB* and *femAB* mutants (containing five, three and one glycine residue in crossbridges, respectively) (Fig. 3a and Supplementary Fig. 6). As expected, binding occurred in a dose-dependent manner and binding to the *femB* mutant was clearly reduced (1.71-fold change), whilst a more drastic reduction in binding was observed with the *femAB* mutant (2.20-fold change). The residual, dose-dependent binding to the *fem* mutant peptidoglycans is in agreement with our identification of a second site recognizing the peptide stems. Fifteen recombinant fusions with mutations in residues previously identified were purified and their binding activity was measured (Fig. 3b,c and Supplementary Fig. 6). Most of the mutations clearly impaired binding to peptidoglycan to a level similar to the level of binding displayed by the WT-mNeonGreen fusion to the *femB* peptidoglycan. The biggest impact on binding was observed with mutations R427M and W489L impairing the recognition of peptide stems (2.47- and 2.18-fold changes as compared to the WT, respectively). These

results therefore confirmed the role of the residues identified by NMR and X-ray crystallography and provided the first evidence that peptide stem recognition by the lysostaphin SH3b domain is critical for binding.

Impact of SH3b mutations on Lss activity

The SH3b mutations previously described (Supplementary Fig. 6) were introduced into the mature lysostaphin enzyme. Recombinant proteins were purified and serial 2-fold dilutions were spotted on agar plates containing autoclaved *S. aureus* cells as a substrate (Supplementary Fig. 7). The enzymatic activity was detected as a clearing zone resulting from the solubilisation of *S. aureus* cell walls. Four independent series of protein purifications were carried out, each including a wild-type lysostaphin protein. One lysostaphin mutant (Lss_M453A) showing an aberrant circular dichroism spectrum could not be analysed; mutant R427M was also excluded from the study as it did not bind to the nickel column. Amongst all the mutations tested, Y472S and W489L led to the most important effects observed (9-fold decrease), whilst all the others had only a limited impact. These results were in line with the binding assays, indicating that no single mutation abolished enzymatic activity and supported our results indicating that the recognition of the peptide stem is equally, if not more, important for binding and activity as is binding to the pentaglycine bridge.

Discussion

The crystal structure reported here shows that SH3b has two well-defined binding sites for *S. aureus* peptidoglycan: a narrow groove that accommodates the G5 lateral chain, with a tightly defined geometry and thus little tolerance for amino acid variants; and a more open site for the P4 peptide stem. One might therefore expect that the specificity for *S. aureus* PG arises entirely from the G5 site, which should be critical for binding. This is not what is indicated by the other results reported here.

The interpretation of CSPs, and of the affinities determined by fitting CSPs to a saturation curve, is more complex than may at first appear. A perturbation of an ^{15}N or ^{1}H nuclear shielding is typically caused by a change in the chemical environment at the nucleus, for example due to a change in hydrogen bonding or a change in the position of neighboring functional groups. Hydrogen bonding is highly directional, implying that an increased mobility of a ligand within its binding site will result in significantly smaller CSPs. Increased mobility will not necessarily result in weaker overall binding, because the loss in enthalpy due to a weaker time-averaged hydrogen bond can easily be compensated by a gain in entropy. Smaller CSPs can therefore indicate a more dynamic binding interaction, rather than simply weaker binding. This phenomenon matches what is observed here (Supplementary Fig. 3). With a simple G5 or P4 ligand that binds in a single site, there are some large CSPs, clearly defining the location of the site (Supplementary Fig. 3a,b). With larger ligands, although the affinity is stronger (implying cooperative binding at both sites, see below), there are fewer large CSP values. The most obvious interpretation is that within each site the ligand has greater mobility, presumably because the physical linkage between the G5 and P4 groups prevents the larger ligands from binding optimally in both sites simultaneously.

There have been many analyses published of binding affinities of ligands that interact via two different sites. A powerful approach is the concept of effective concentration [24,25]. Consider a ligand L1-L2 that binds at two sites, R1 and R2, with a flexible linker between L1 and L2 (Fig 4a). If the ligand detaches from site R2, then the rate at which L2 rebinds at R2 is given by $k_{on}\times[L2]_{eff}$, where k_{on} is the rate constant for binding and $[L2]_{eff}$ is the effective concentration of L2 at the R2 binding site (Fig 4b). For a short linker with optimal length and geometry, $[L2]_{eff}$ can be orders of magnitude larger than [L2], leading to much stronger binding than would be seen in the absence of L1 (because the overall affinity for L2 is equal to the off-rate divided by the on-rate, and we can assume that the off-rate is unaffected by the presence of the linker): in other words, to cooperative binding, such that the affinity for the intact ligand L1-L2 is much stronger than the affinity for L1 or L2 alone. Conversely, if the linker is too short

(Fig 4c), then L2 is unable to reach R2, and $[L2]_{eff}$ is smaller than [L2], leading to a complete lack of cooperativity. If the binding sites R1 and R2 allow for some flexibility in geometry, then we may have a situation as shown in Fig 4d, where binding of the ligand can be achieved by allowing some mobility in the bound conformation at the cost of suboptimal binding geometry. The cooperativity will not be as great as it would be with ideal geometry and thus the affinity will be stronger but not by a large amount. This appears to be exactly the situation observed here: affinity is 10× stronger, but CSPs are smaller. Furthermore, single site mutations have relatively little effect on the affinity or on enzymatic activity, suggesting that the exact shape or complementarity of the binding site is relatively unimportant, consistent with this model.

It is a legitimate question to ask why SH3b should have evolved separate binding sites for G5 and P4, but located on the protein surface in such a way that simultaneous binding to both sites is not possible. What is the biological advantage? Our data, and the interpretation derived here, provide suggestions. The function of the SH3b domain is to attach lysostaphin to PG, in such a way as to increase access of the catalytic domain to its G5 substrate. It is therefore not desirable for the affinity for PG to be too strong, otherwise SH3b would detach too slowly and not allow the catalytic domain to move from one G5 substrate to another. A good solution is to have two binding sites, both with weak affinity and thus rapid off-rates, and organised so as to provide a moderate degree of cooperativity in binding to the complex substrate. This allows the protein to 'walk' around the PG surface, continually keeping at least one site bound, but permitting rapid searching on the PG surface. A very similar solution has been adopted by a number of cellulases, which have two different cellulose binding domains arranged in tandem [26-29].

A comparison of interactions at the two sites with different ligands (Fig. 1) suggests that the larger ligands have weaker interactions at the G5 site, since the G5 interactions (red) decrease more than do the P4 interactions (green). This result is at first sight counterintuitive, because the lysostaphin catalytic domain specifically targets G5. However SH3b should not bind too tightly to G5, because otherwise it would block access of the catalytic domain. It therefore makes sense for the larger (and thus more cell-wall-like) fragments to favor binding of the peptide stem, as long as some specificity for G5 is maintained, and as long as SH3b is not locked into binding at any particular location. We may therefore describe the role of SH3b as to contribute to the initial (weak) binding of the enzyme on the PG surface. This conclusion is also consistent with the observation that the mutations more critical to binding affinity are found in the P4 site, not the G5 site. Surprisingly, and in agreement with this result, the SH3b

domain still binds in a dose-dependent manner to the *femAB* peptidoglycan, containing crossbridges made of a single glycine residue. This suggests that the recognition of the pentaglycine stem is not essential for the binding of the enzyme with its substrate. Based on this result, it is tempting to hypothesize that the catalytic activity of lysostaphin rather than the binding itself is the major determinant for the specific hydrolysis of staphylococcal peptidoglycan. In *Staphylococcus carnosus*, the *femB* mutation is associated with a 3000-fold increase in the MIC values for lysostaphin from 0.01 to 32 µg/ml [30]. Given the limited impact of the SH3b mutations on binding, this result suggests that the high resistance to lysostaphin in the *femB* mutant is not caused by the slight difference in binding activity of the penta- vs tri-glycine interpeptide bridge, but is mainly due to the decreased enzymatic activity of lysostaphin.

The networks of contacts between ligand and two sets of SH3 domains strongly suggest that our two-site model for P4-G5 (and therefore true, complex sacculus ligand) is physiologically relevant. The observed pocket for the terminal P4 D-Ala is highly complementary in both shape and contact type; a lack of adjoining pocket for a second D-Ala of a pentapeptide is in keeping with the dominance of tetrapeptides in staphylococcal peptidoglycan [31]. Residues responsible for P4 recognition are conserved in several homologues present in the PDB despite the relative low sequence identity across the entire domain – *S. capitis* ALE-1 (code 1R77, 83% sequence identity, [19]), *Staphylococcus* phage GH15 lysin (2MK5, 49%, [32]) and phage phi7917 lysin (5D76, 30%, unpublished). These related structures have features that validate our identification of the P4 binding site (overlays shown in Supplementary Fig. 4): in ALE-1 a purification tag places a lysine in an identical position to the K3 crosslink, and in phi7917 a muramyldipeptide cleavage product has bound in this region. Our identification of a "second" binding site supplementing the "traditional" pentaglycine cleft may have implications for other SH3b and SH3-like domains that are used in varying architectures to recognize peptidoglycan in organisms that do not utilize the G5 crossbridge.

No major difference exists between the structure of the SH3b domain in its apo form (4LXC) and in complex with the P4-G5 ligand (this work), suggesting that the ligand displays a dynamic structure to "fit" within the binding clefts present on the SH3b domain. Previous NMR studies support this idea and have shown that the D-Lac, L-Ala, and D-Glu adopt a limited number of conformers, whereas the L-Lys-D-Ala termini are disordered (with no NOE contacts observed [33]). Further relaxation measurements using the P4-G5 ligand could be carried out to test this hypothesis but it appears difficult to extrapolate relaxation experiments to a complex molecule such as peptidoglycan.

334 The data presented here provide an explanation as to why the binding activity of the SH3b
335 domain of lysostaphin is not affected by exogenous pentaglycine or its own catalytic
336 products [21]; our model suggests that the muropeptide interactions are only satisfied when
337 presented by non-contiguous epitopes of mature, physiological peptidoglycan. The location of
338 these sites on different faces of the SH3b molecule ensures that both are unlikely to be
339 contacted by a soluble, torsionally less-restricted fragment. We hypothesize that this will be an
340 excellent method for processive degradation of the peptidoglycan.
341 The structure of the SH3b domain in complex with the P4-G5 peptide shed light on the NMR
342 analyses previously published [34] and those described in this manuscript, revealing the existence
343 of two independent binding sites on opposite sides of the SH3b domain. The binding
344 mechanism described here is consistent with the formation of large protein aggregates during
345 titration with complex PG fragments. Recognition of the same PG peptide stem by independent
346 SH3b domains (referred to as "clustering") leads to an effective increase in enzyme
347 concentration at the cell surface. In agreement with this hypothesis, the direct observation of
348 *S. aureus* cell wall digestion by lysostaphin using atomic force microscopy revealed the
349 existence of nanoscale perforations that precede cell lysis [35].
350

Materials and methods

Bacterial strains, plasmids and growth conditions.

Bacterial strains and plasmids used in this study are described in Supplementary Table 3. *E. coli* Lemo21 (DE3) and NEB5α strains were grown at 37°C in Luria-Bertani (LB) or M9 minimal medium containing 1 g/L of $^{15}NH_4Cl$ (and 2 g/L $^{13}C_6$-glucose where necessary), supplemented with ampicillin at a concentration of 100 µg/ml.

Construction of recombinant plasmids for protein production.

Both plasmids expressing the full length lysostaphin (pET-Lss) and the SH3b domains with a non-cleavable N-terminal His-tag for NMR studies (pET-SH3b) have been previously described [36,37]. The plasmid encoding the SH3b-mNeonGreen fusion (pET-SH3b-NG) was constructed by Gibson assembly using a DNA synthetic fragment (Integrated DNA Technology) cloned into the vector pET2818 cut with NcoI and BamHI. Plasmid pET-SH3b-TEV used to produce the SH3b domain without a tag for X-ray crystallography was constructed by Gibson assembly using a synthetic DNA fragment (Integrated DNA Technology) cloned into pET2817 digested with NcoI and BamHI. The amino acid sequences of the wild-type recombinant proteins are described in Supplementary Fig 8.

Site-directed mutagenesis.

Mutagenesis of plasmids pET-SH3b and pET-Lss was performed using the GeneArt® Site-Directed Mutagenesis System (Thermo Fisher Scientific). All primers used in this study are described in the Supplementary Table 4. The same pair of oligonucleotides was used to introduce mutations in both plasmids, except for mutations N405D and W489L which required distinct pairs of oligonucleotides to build mNeonGreen fusions and lysostaphin mutants.

Purification of recombinant Lss protein and Lss-SH3b protein domains.

Cells were grown to an optical density at 600nm (OD_{600}) of 0.7 in LB or M9 media for NMR analyses and protein production was induced by the addition of 1 mM IPTG. After 4h, induced cells were harvested and resuspended in buffer A (50 mM Tris-HCl, 500m M NaCl, pH 8.0) and crude lysates were obtained by sonication (3 × 30s, 20% output; Branson Sonifier 450). Soluble proteins were loaded onto a HiTrap IMAC column (GE Healthcare, Uppsala, Sweden) charged with Ni^{2+} or Zn^{2+} ions for SH3b (alone or fused to mNeonGreen) and full-length

lysostaphin, respectively. His-tagged proteins were eluted with a 20 column volume linear gradient of buffer B (500 mM imidazole, 50 mM Tris-HCl, 500 mM NaCl, pH 8.0). Recombinant His-tagged proteins were concentrated and purified by size-exclusion chromatography on a Superdex 75 HR column (GE Healthcare, Uppsala, Sweden). For NMR experiments, proteins were purified using 50 mM Na_2HPO_4 (pH 6.0). All purified proteins were analysed by SDS-PAGE.

For crystallography experiments, the SH3b domain was produced using plasmid pET-SH3b-TEV. The N-terminal tag was removed using recombinant TEV protease (0.5 mg of TEV per mg of SH3b protein). Digestions were performed at 37°C overnight in buffer C (150 mM NaCl, 50 mM Tris-HCl, pH 8.35). Following digestion, proteins were loaded onto a HiTrap IMAC column, and cleaved SH3b proteins were recovered in the flow through. Proteins concentrations were determined using absorbance at 280 nm.

The characterization of all recombinant proteins is described in the supplementary information section (Supplementary Fig. 8-12).

Purification of *S. aureus* PG sacculi

PG sacculi were isolated from exponentially growing *S. aureus* cells as previously described [38]. Pure PG was freeze-dried and resuspended at a final concentration of 25 mg/ml.

Peptidoglycan digestions for NMR titration assays

S. aureus PG was digested with mutanolysin (Sigma). To purify PG dimers (GM-P5-G5-GM-P4-G5), 180 mg of PG were digested with 2.5 mg of mutanolysin in a final volume of 5 ml using 20 mM phosphate buffer (pH 6.0). After overnight incubation the enzyme was heat-inactivated. Half of the sample was used to purify dimers. The pH of the other half of digestion was adjusted to 7.5 and it was further digested with 2 mg of EnpA to generate disaccharide-peptides. EnpA was heat-inactivated.

Purification of peptidoglycan fragments by rp-HPLC

Prior to rp-HPLC analysis and fractionation, soluble peptidoglycan fragments were reduced with sodium borohydride to eliminate double peaks corresponding to the α-and β-anomers as previously described [38]. Fractionation of material corresponding to the digestion of 50 mg of PG was carried out on a Hypersil GOLD aQ column (C18; 21 × 250 mm, Thermo Scientific) and separated at a flow rate of 10 ml/min using 10 mM ammonium phosphate (pH 5.5) as a

mobile phase (buffer A). After a short isocratic step (2 column volumes), PG fragments were eluted with a 15 column volume methanol linear gradient (0 to 30%) in buffer A. Individual peaks were collected, freeze-dried and analysed by mass spectrometry. The fractions corresponding to the major dimer (GM-P5-G5-GM-P4-G5) were desalted by HPLC using a water-acetonitrile gradient, freeze-dried and resuspended in MilliQ water.

Production of peptidoglycan fragments by chemical synthesis

The tetrasaccharide (GMGM) was described previously [39]. All peptides and branched peptides (>95% purity) were purchased from Peptide Protein Research Ltd. (UK) Purity was assessed by HPLC and mass spectrometry. The characterization of all ligands is described in the supplementary information section. The pentaglycine peptide was purchased from SIGMA Aldrich (ref. G5755).

Crystallography and structure determination

Crystallisation was initiated via standard screening in sitting drop 96-well clover-leaf crystallography trays at 18 mg/ml with 3.41 mM AγQK[GGGGG]A in a 1:2 drop ratio of screening agent to protein solution. The trays were incubated at 18 °C. Tetragonal bipyramidal crystals formed within the first 48 hours in 100 mM Bis-tris pH 5.5, 25% (w/v) poly-ethylene glycol 3350 and 200 mM ammonium sulphate.

Crystals were cryo-protected using the above conditions (inclusive of AγQK[GGGGG]A to maintain the ligand:protein complex), and an additional 20% v/v ethylene glycol. Two datasets were collected (Supplementary Table 5): a high resolution set at the I03 beamline, Diamond Light Source, Oxford, and a second set on a Rigaku Micromax home source. Data were processed with XiaII/XDS [40]. The B-factors for the high-resolution set are higher than expected, but match that of the Wilson B, and the dataset has a normal intensity distribution. An initial model was solved using the existing apo structure 5LEO [20] as a molecular replacement model in PHASER [41], and the corresponding structure autobuilt using PHENIX [42], with the ligand added via visual inspection of the difference map. The structure was updated and refined using COOT [43], PHENIX [42] and PDB-redo [44], resulting in a final structure with an R/Rfree of 19.9%/23.0%.

NMR experiments

NMR experiments were conducted on Bruker Avance I 800 and DRX-600 spectrometers at 298K. 2D NHSQC experiments were carried out using the b_hsqcetf3gpsi pulse program

(Bruker) with relaxation delay 1 s, 128 complex increments (ca. 1 h 18 m per spectrum). Lss-SH3b proteins were quantified by measuring the absorbance at 280 nm and adjusted to a concentration of 60 µM in 50 mM Na_2HPO_4 (pH 6.0). All ligands were quantified by NMR based on the intensity of methyl protons using trimethylsilylpropanoic acid (TSP) as a standard. ^{15}N HSQC experiments and chemical shift perturbation (CSP) analyses were performed as previously described [39].

PG binding assays

The PG binding activity of SH3b domains was studied using in-gel fluorescence. Protein amounts equivalent to 3 µg of the wild-type recombinant SH3b-mNeonGreen were adjusted based on the fluorescence intensity of the bands corresponding to the full length proteins. Following incubation in the presence of increasing amounts of PG (0-400 µg) in a final volume of 40 µl for 20 min at room temperature, PG and bound proteins were pelleted at 17,000 × g for 5 minutes. Twenty µl of supernatant corresponding to unbound proteins were loaded on an SDS-PAGE and scanned using a BioRad Chemidoc XRS+ system. Fluorescence intensity was quantified using the ImageJ software. The percentage of binding was determined using the signal intensity measured in the absence of PG as a reference.

Lysostaphin activity assays

S. aureus SH1000 [45] was grown to an optical density OD_{600} of 1.0. Cells were harvested, resuspended in distilled water, autoclaved and incorporated in agar plates at a final OD_{600} of 0.5. Five µl corresponding to serial dilutions of the recombinant lysostaphin proteins were spotted on the plates containing autoclaved cells as a substrate and incubated overnight at 37 °C. Lytic activities were detected as clearing zones and compared by determining the lowest amount of enzyme giving a detectable digestion of the substrate

Data availability

Structural data have been deposited in the Protein DataBank (PDB) with coordinate accession numbers 6RK4 (high-resolution set) and 6RJE (home source set). All other data generated or analyzed during this study are included in this published article (and its supplementary information files) or are available from the corresponding authors on reasonable request."

References

1. Schindler, C.A. & Schuhardt, V.T. Lysostaphin: a new bacteriolytic agent for the *Staphylococcus*. *Proc Natl Acad Sci U S A* **51**, 414-21 (1964).
2. Schindler, C.A. & Schuhardt, V.T. Purification and properties of Lysostaphin--a lytic agent for *Staphylococcus aureus*. *Biochim Biophys Acta* **97**, 242-50 (1965).
3. Thumm, G. & Götz, F. Studies on prolysostaphin processing and characterization of the lysostaphin immunity factor (Lif) of *Staphylococcus simulans* biovar *staphylolyticus*. *Mol Microbiol* **23**, 1251-65 (1997).
4. Wu, J.A., Kusuma, C., Mond, J.J. & Kokai-Kun, J.F. Lysostaphin disrupts *Staphylococcus aureus* and *Staphylococcus epidermidis* biofilms on artificial surfaces. *Antimicrob Agents Chemother* **47**, 3407-14 (2003).
5. Climo, M.W., Patron, R.L., Goldstein, B.P. & Archer, G.L. Lysostaphin treatment of experimental methicillin-resistant *Staphylococcus aureus* aortic valve endocarditis. *Antimicrob Agents Chemother* **42**, 1355-60 (1998).
6. Dajcs, J.J. *et al.* Lysostaphin treatment of methicillin-resistant *staphylococcus aureus* keratitis in the rabbit. *Am J Ophthalmol* **130**, 544 (2000).
7. Johnson, C.T. *et al.* Hydrogel delivery of lysostaphin eliminates orthopedic implant infection by *Staphylococcus aureus* and supports fracture healing. *Proc Natl Acad Sci U S A* **115**, E4960-E4969 (2018).
8. Kiri, N., Archer, G. & Climo, M.W. Combinations of lysostaphin with beta-lactams are synergistic against oxacillin-resistant *Staphylococcus epidermidis*. *Antimicrob Agents Chemother* **46**, 2017-20 (2002).
9. Kokai-Kun, J.F., Chanturiya, T. & Mond, J.J. Lysostaphin as a treatment for systemic *Staphylococcus aureus* infection in a mouse model. *J Antimicrob Chemother* **60**, 1051-9 (2007).
10. Kokai-Kun, J.F., Walsh, S.M., Chanturiya, T. & Mond, J.J. Lysostaphin cream eradicates *Staphylococcus aureus* nasal colonization in a cotton rat model. *Antimicrob Agents Chemother* **47**, 1589-97 (2003).
11. Satishkumar, R. *et al.* Evaluation of the antimicrobial activity of lysostaphin-coated hernia repair meshes. *Antimicrob Agents Chemother* **55**, 4379-85 (2011).
12. Blazanovic, K. *et al.* Structure-based redesign of lysostaphin yields potent antistaphylococcal enzymes that evade immune cell surveillance. *Mol Ther Methods Clin Dev* **2**, 15021 (2015).
13. Zhao, H. *et al.* Depletion of T cell epitopes in lysostaphin mitigates anti-drug antibody response and enhances antibacterial efficacy *in vivo*. *Chem Biol* **22**, 629-39 (2015).
14. Liu, Y. *et al.* Immunomimetic designer cells protect mice from MRSA infection. *Cell* **174**, 259-270 e11 (2018).
15. Raz, A., Serrano, A., Thaker, M., Alston, T. & Fischetti, V.A. Lysostaphin lysibody leads to effective opsonization and killing of methicillin-resistant *Staphylococcus aureus* in a murine model. *Antimicrob Agents Chemother* **62:e01056-18.**(2018).
16. Wall, R.J. *et al.* Genetically enhanced cows resist intramammary *Staphylococcus aureus* infection. *Nat Biotechnol* **23**, 445-51 (2005).
17. Wittekind, M. & Schuch, R. Cell wall hydrolases and antibiotics: exploiting synergy to create efficacious new antimicrobial treatments. *Curr Opin Microbiol* **33**, 18-24 (2016).
18. Baba, T. & Schneewind, O. Target cell specificity of a bacteriocin molecule: a C-terminal signal directs lysostaphin to the cell wall of *Staphylococcus aureus*. *Embo J* **15**, 4789-97 (1996).
19. Lu, J.Z., Fujiwara, T., Komatsuzawa, H., Sugai, M. & Sakon, J. Cell wall-targeting domain of glycylglycine endopeptidase distinguishes among peptidoglycan cross-bridges. *J Biol Chem* **281**, 549-58 (2006).
20. Mitkowski, P. *et al.* Structural bases of peptidoglycan recognition by lysostaphin SH3b domain. *Sci Rep* **9**, 5965 (2019).

21. Gründling, A. & Schneewind, O. Cross-linked peptidoglycan mediates lysostaphin binding to the cell wall envelope of *Staphylococcus aureus*. *J Bacteriol* **188**, 2463-72 (2006).
22. Tamai, E. *et al.* X-ray structure of a novel endolysin encoded by episomal phage phiSM101 of *Clostridium perfringens*. *Mol Microbiol* **92**, 326-37 (2014).
23. Shaner, N.C. *et al.* A bright monomeric green fluorescent protein derived from *Branchiostoma lanceolatum*. *Nat Methods* **10**, 407-9 (2013).
24. Williamson, M.P. *How proteins work*, 464 (Garland Science, New York, 2011).
25. Zhou, H.X. Quantitative relation between intermolecular and intramolecular binding of pro-rich peptides to SH3 domains. *Biophys J* **91**, 3170-81 (2006).
26. Bolam, D.N. *et al. Pseudomonas* cellulose-binding domains mediate their effects by increasing enzyme substrate proximity. *Biochem J* **331 (Pt 3)**, 775-81 (1998).
27. Gill, J. *et al.* The type II and X cellulose-binding domains of *Pseudomonas* xylanase A potentiate catalytic activity against complex substrates by a common mechanism. *Biochem J* **342 (Pt 2)**, 473-80 (1999).
28. Nagy, T. *et al.* Characterization of a double dockerin from the cellulosome of the anaerobic fungus *Piromyces equi*. *J Mol Biol* **373**, 612-22 (2007).
29. Raghothama, S. *et al.* Characterization of a cellulosome dockerin domain from the anaerobic fungus *Piromyces equi*. *Nat Struct Biol* **8**, 775-8 (2001).
30. Nega, M. *et al.* Secretome analysis revealed adaptive and non-adaptive responses of the *Staphylococcus carnosus femB* mutant. *Proteomics* **15**, 1268-79 (2015).
31. Gally, D. & Archibald, A.R. Cell wall assembly in *Staphylococcus aureus*: proposed absence of secondary crosslinking reactions. *J Gen Microbiol* **139**, 1907-13 (1993).
32. Gu, J. *et al.* Structural and biochemical characterization reveals LysGH15 as an unprecedented "EF-hand-like" calcium-binding phage lysin. *PLoS Pathog* **10**, e1004109 (2014).
33. Meroueh, S.O. *et al.* Three-dimensional structure of the bacterial cell wall peptidoglycan. *Proc Natl Acad Sci U S A* **103**, 4404-9 (2006).
34. Tossavainen, H. *et al.* Structural and Functional Insights Into Lysostaphin-Substrate Interaction. *Front Mol Biosci* **5**, 60 (2018).
35. Francius, G., Domenech, O., Mingeot-Leclercq, M.P. & Dufrêne, Y.F. Direct observation of *Staphylococcus aureus* cell wall digestion by lysostaphin. *J Bacteriol* **190**, 7904-9 (2008).
36. Jagielska, E., Chojnacka, O. & Sabala, I. LytM fusion with SH3b-like domain expands its activity to physiological conditions. *Microb Drug Resist* **22**, 461-9 (2016).
37. Sabala, I. *et al.* Crystal structure of the antimicrobial peptidase lysostaphin from *Staphylococcus simulans*. *FEBS J* **281**, 4112-22 (2014).
38. Mesnage, S., Chau, F., Dubost, L. & Arthur, M. Role of *N*-acetylglucosaminidase and *N*-acetylmuramidase activities in *Enterococcus faecalis* peptidoglycan metabolism. *J Biol Chem* **283**, 19845-53 (2008).
39. Mesnage, S. *et al.* Molecular basis for bacterial peptidoglycan recognition by LysM domains. *Nat Commun* **5**, 4269 (2014).
40. Kabsch, W. Xds. *Acta Crystallogr D Biol Crystallogr* **66**, 125-32 (2010).
41. McCoy, A.J. *et al.* Phaser crystallographic software. *J Appl Crystallogr* **40**, 658-674 (2007).
42. Zwart, P.H. *et al.* Automated structure solution with the PHENIX suite. *Methods Mol Biol* **426**, 419-35 (2008).
43. Emsley, P. & Cowtan, K. Coot: model-building tools for molecular graphics. *Acta Crystallogr D Biol Crystallogr* **60**, 2126-32 (2004).
44. Joosten, R.P., Joosten, K., Cohen, S.X., Vriend, G. & Perrakis, A. Automatic rebuilding and optimization of crystallographic structures in the Protein Data Bank. *Bioinformatics* **27**, 3392-8 (2011).

45. Horsburgh, M.J. *et al. sigmaB* modulates virulence determinant expression and stress resistance: characterization of a functional rsbU strain derived from *Staphylococcus aureus* 8325-4. *J Bacteriol* **184**, 5457-67 (2002).

Acknowledgments

LSG is a PhD student funded by the Mexican government through a CONACYT scholarship. HWM is supported by a BBSRC MIBTP studentship. We thank BBSRC and EPSRC for funding to upgrade the 600 and 800 MHz spectrometers, respectively (grant numbers BB/R000727/1 and EP/S01358X/1). The work in IS laboratory is supported by the Foundation for Polish Science (FNP) programme, co-financed by the European Union under the European Regional Development Fund, grant TEAMTECH/2016-3/19.

Authors' contribution

SM conceived the project and designed experiments with MPW and ALL. AMH and AJR assigned the SH3b spectrum. LSG carried out all NMR experiments and analysed them with the help of AMH and MPW. BS and LSG built all SH3b recombinant proteins to carry out functional assays and crystallographic analyses. AWM crystallised the protein and solved the structure with the help of ALL. EJ and IS provided reagents. LSG, HWM, BS, AMH, MPW, ALL and SM analyzed the data. LSG, SM, ALL and MPW wrote the manuscript.

603 **Figure legends**

604

605 **Figure 1. Mapping the interaction surface of the SH3b domain with synthetic *S. aureus***
606 **PG fragments**

607 For each NMR titration, the average CSP was calculated and two-fold average CSP was chosen
608 as a threshold to identify surface residues interacting with ligands. The residues interacting
609 with the pentaglycine crossbridges are highlighted in red, those interacting with the peptide
610 stem in green. Interaction maps corresponding to six ligands are shown. **a**, G5 peptide; **b**, P4;
611 **c**, P4-G5; **d**, P5-G5-P4; **f**, GM-P5-G5-GM-P4-G5. Titrations confirmed the existence of a
612 narrow cleft previously proposed to bind the PG crossbridges [19] and recently shown to interact
613 with pentaglycine [20]. They also revealed a set of residues interacting with the peptide stem,
614 located on the face of the protein opposite to the G5 binding cleft.

615

616 **Figure 2. Structure of lysostaphin SH3b in complex with the P4-G5 ligand**

617 The SH3b domain and a symmetry-related partner are coloured white and blue, respectively;
618 ligand is coloured by atom type, with P4 C atoms green and G5 C atoms pink. **a**, protein fold
619 with termini labelled, and two representations (fold and ligand in ribbon/stick and surface
620 formats). **b**, Co-crystal structure showing the SH3b:ligand shape complementarity. **c**, Rotated
621 view of a single SH3b domain showing the interaction with the P4 ligand (blue, with peptide
622 units labelled 1-4). **d**, experimental 2Fo-Fc difference map contoured at 1 σ for different
623 regions of the bound ligand, with selected interacting residues in stick form. The L-Ala 1 end
624 panel is from the 2.5 Å dataset, others are from the 1.4 Å form. Residues from the symmetry-
625 related SH3b domain are denoted by use of a prime (‘), and hydrogen bonds represented as a
626 dashed line.

627

628 **Figure 3. Binding activity of recombinant SH3b-mNeonGreen (SH3b-NG) proteins to**
629 **purified *S. aureus* peptidoglycan**

630 **a,** peptidogycan binding activities of WT SH3b-NG on *S. aureus* WT and *fem* mutants with an
631 altered peptidoglycan crossbridge. **b**, peptidogycan binding activities of WT SH3b-NG and
632 derivatives with mutations in residues involved in the interaction with the G5 ligand. **c**,
633 peptidoglycan binding activities of WT SH3b-NG and derivatives with mutations in residues
634 involved in the interaction with the P4 ligand. The graphs show dose-binding responses whilst
635 Supplementary Table 2 indicates the amount of PG required for 50% binding (PG_{50}) and the

636 corresponding fold change compared to the amount of PG required for 50% binding of the WT
637 protein as a reference.
638
639 **Figure 4. Models for binding of a ligand at two sites**
640 **a**, schematic representation of a receptor with two sites (R1 and R2), which bind the L1 and L2
641 ligand sites respectively. L1 and L2 are connected by a flexible linker. **b**, the flexibility of the
642 linker allows the R1 site to stay attached, but the R2 site to detach. The effective concentration
643 of L2 at the R2 site (and thus the cooperativity of binding) will depend on the length and
644 flexibility of the linker. **c**, if the linker is too short, it is not possible for the ligand to bind
645 simultaneously at both R1 and R2. It can alternate between both sites, which will still result in
646 cooperative binding, though less than in case **b**. **d**, a weaker enthalpy of binding (for example
647 due to the shortness of the linker preventing optimal binding at both sites) can to some extent
648 be compensated by greater entropy (increased relative motion of ligand and receptor) if there
649 is weak binding in non-optimal positions.

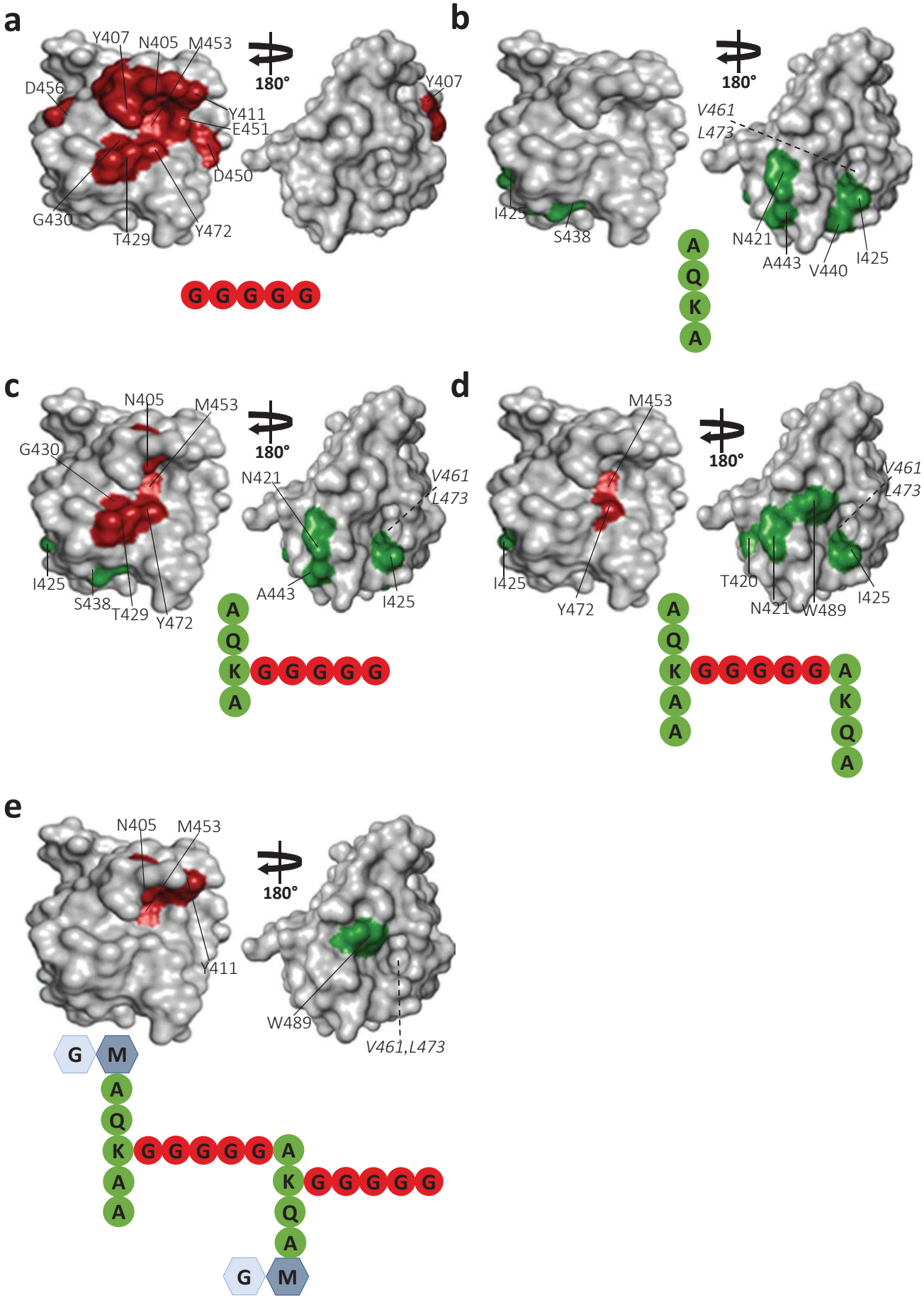
a
Y407
N405
M453
D456
Y411
E451
D450
G430
T429
Y472
180°
Y407
G G G G G
b
180°
V461
L473
I425
S438
N421
A443
V440
I425
A
Q
K
A
c
N405
M453
G430
I425
S438
T429
Y472
180°
N421
V461
L473
A443
I425
A
Q
K
G G G G G
A
d
M453
I425
Y472
180°
V461
L473
T420
N421
W489
I425
A
Q
K
G G G G G
A
K
Q
A
A
A
e
N405
M453
Y411
180°
W489
V461,L473
G
M
A
Q
K
G G G G G
A
A
A
K
G G G G G
Q
A
G
M

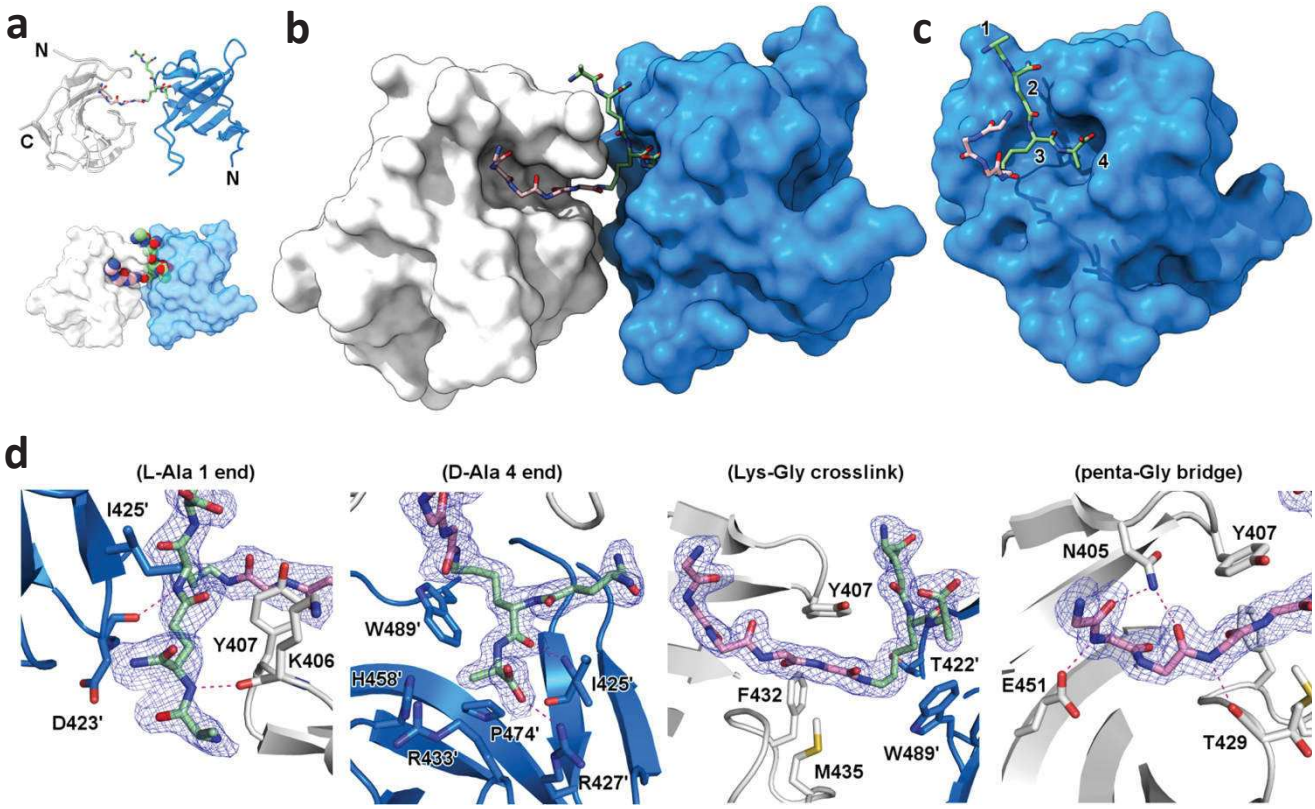
a
N
C
N
b
c
1
2
3
4
d
(L-Ala 1 end)
I425'
Y407
K406
D423'
(D-Ala 4 end)
W489'
H458'
I425'
P474'
R433'
R427'
(Lys-Gly crosslink)
Y407
T422'
F432
W489'
M435
(penta-Gly bridge)
N405
Y407
E451
T429

Figure 2

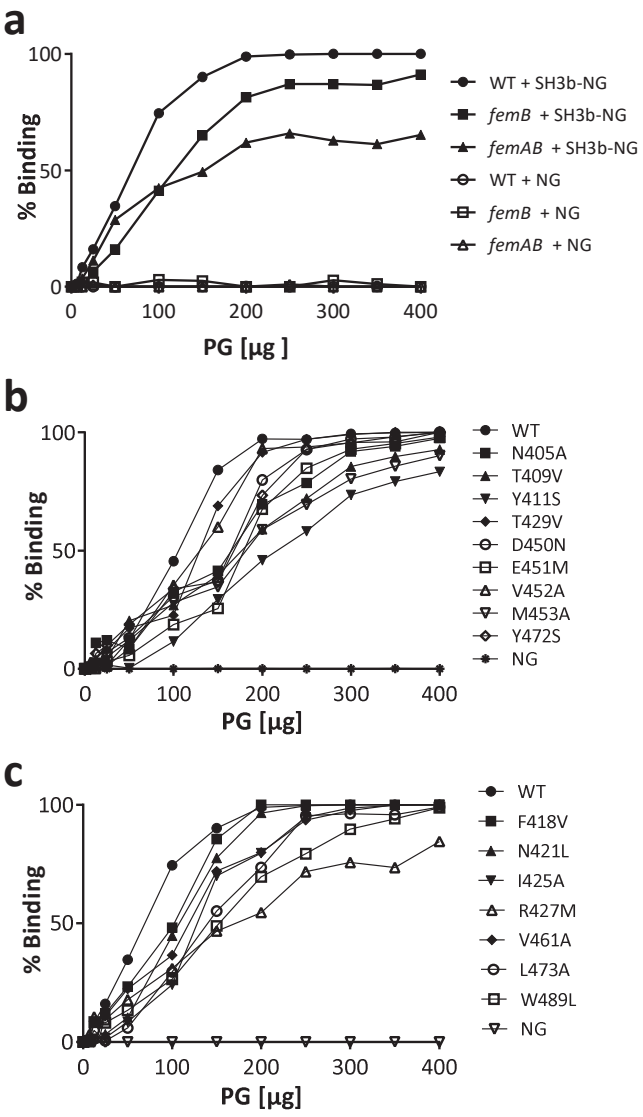
a
100
50
0
% Binding
0
100
200
300
400
PG [µg]
WT + SH3b-NG
femB + SH3b-NG
femAB + SH3b-NG
WT + NG
femB + NG
femAB + NG
b
100
50
0
% Binding
0
100
200
300
400
PG [µg]
WT
N405A
T409V
Y411S
T429V
D450N
E451M
V452A
M453A
Y472S
NG
c
100
50
0
% Binding
0
100
200
300
400
PG [µg]
WT
F418V
N421L
I425A
R427M
V461A
L473A
W489L
NG

Figure 3

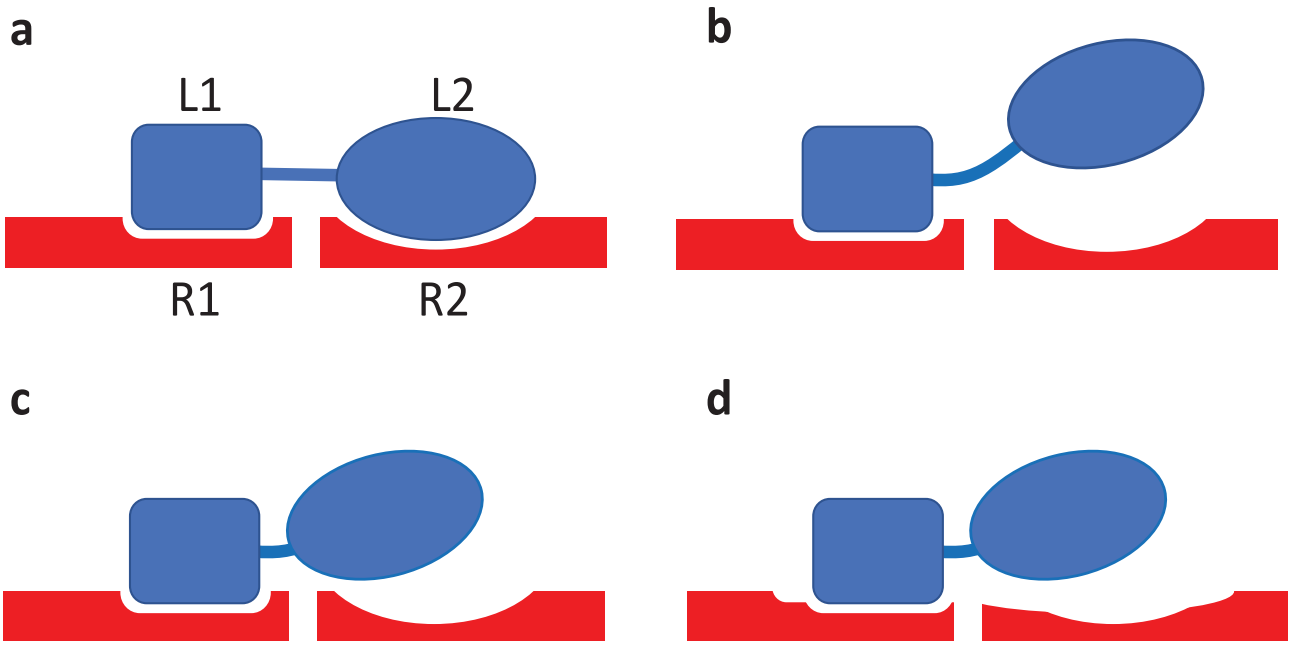

Figure 4

Supplementary Table 1. CSPs associated with amino-acid side-chains.

G5			P4		
Side chain	**Normalized Δδ[a] (ppm)**	**Δδ/averageΔδ[b] (0.016)[c]**	**Side chain**	**Normalized Δδ[a] (ppm)**	**Δδ/averageΔδ[b] (0.079)[c]**
Ws402	0.006	0.383	Ws402	0.039	0.489
N405s	0.122	7.643	N405s	0.028	0.350
Ws460	0.005	0.288	Rs427	0.168	2.122
Ws478	0.004	0.258	Rs433	0.048	0.610
Ws489	0.001	0.068	Ws460	0.143	1.796
			Rs470	0.038	0.484
			Rs476	0.015	0.194
			Ws478	0.014	0.175
			Ws489	0.157	1.982
P4-G5			**GM-P4-G5**		
Side chain	**Normalized Δδ[a] (ppm)**	**Δδ/averageΔδ[b] (0.069)[c]**	**Side chain**	**Normalized Δδ[a] (ppm)**	**Δδ/averageΔδ[b] (0.121)[c]**
Ws402	0.010	0.143	Ws402	0.126	1.045
N405s	*	*	N405s	0.174	1.446
Rs427	*	*	Rs427	0.226	1.873
Rs433	0.024	0.348	Rs433	0.096	0.794
Ws460	0.129	1.879	Ws460	0.199	1.648
Rs470	0.231	3.367	Rs470	0.216	1.786
Rs476	0.012	0.175	Rs476	0.071	0.588
Ws478	0.004	0.058	Ws478	0.021	0.171
Ws489	0.097	1.417	Ws489	0.143	1.188
P5-G5-P4-G5			**GM-P5-G5-GM-P4-G5**		
Side chain	**Normalized Δδ[a] (ppm)**	**Δδ/averageΔδ[b] (0.119)[c]**	**Side chain**	**Normalized Δδ[a] (ppm)**	**Δδ/averageΔδ[b] (0.057)[c]**
Ws402	0.059	0.499	Ws402	0.015	0.256
N405s	0.078	0.653	N405s	0.191	3.343
Rs427	0.244	2.059	Rs427	0.071	1.247
Rs433	0.132	1.108	Rs433	0.013	0.235
Ws460	0.189	1.597	Ws460	0.066	1.165
Rs470	0.083	0.703	Rs470	0.019	0.334
Rs476	0.032	0.272	Rs476	0.029	0.513
Ws478	0.172	1.452	Ws478	0.053	0.925
Ws489	0.095	0.802	Ws489	0.039	0.689

[a] Nor malized ^{1}H and ^{15}N chemical shifts in ppm.
[b] Value for the ^{1}H ^{15}N chemical shift divided by the average chemical shift.
[c] Average chemical shift value from all residues when titrated with the corresponding ligand.
*Slow conformational exchange was reported for the backbone and side-chain of these residues showing line broadening and disappearance of the signal at the highest ligand concentrations.

Supplementary Table 2. Peptidoglycan binding activities of WT SH3b-NG and derivatives showing the amount of PG required for 50% binding (PG_{50}) and the fold change as compared to the wild-type domain.

	SH3b	PG_{50}	Fold change
Fig. 3a	WT [c]	69.2	1.00
	femB	118.3	1.71
	femAB	152.6	2.20
Fig. 3a	WT	105.8	1.00
	N405A	163.0	1.54
	T409V	167.3	1.58
	Y411S	193.5	1.83
	T429V	129.5	1.22
	D450N	164.8	1.56
	E451M	177.9	1.68
	V452A	129.7	1.23
	M453A	171.5	1.62
	Y472S	168.0	1.59
Fig. 3c	WT	69.2	1.00
	F418V	102.4	1.48
	N421L	107.9	1.56
	V461A	118.9	1.72
	I425A	128.1	1.85
	R427M	170.6	2.47
	L473A	139.0	2.01
	W489L	151.0	2.18

Table 3. Bacterial strains and plasmids used in this study

Strains, plasmids	Relevant properties or genotype[a]	Source or reference
Strains		
Staphylococcus aureus		
SH1000	8325-4 derivate with a restored *rsbU* allele	46
NCTC8325	Wild type strain	46
Escherichia coli		
Lemo21(DE3)	BL21 derivative for protein production	NEB
NEB5α	Host strain for DNA cloning	NEB
Plasmids		
pET15b	Plasmid for the production of proteins with an N-terminal His-tag	Novagen
pET21a	Plasmid for the production of proteins with a C-terminal His-tag	Novagen
pET2818	Plasmid for the production of proteins with a C-terminal His-tag	lab stock
pET2817-TEV	Plasmid for the production of proteins with an N-terminal cleavable His-tag	lab stock
pET- SH3b	pET15b derivative encoding Lss SH3b domain for NMR experiments	38
pET-Lss	pET21a derivative for the expression of the full length Lss lysostaphin	39
pET-SH3b-TEV	pET2817-TEV derivative for the expression of the Lss-SH3b domain for X-ray crystallography	This study
pET-SH3b-NG	pET2818 derivative for the expression of SH3b-mNeonGreen fusions	This study

[a] Amp^R, resistant to ampicillin; Erm^R, resistant to erythromycin

Supplementary Table 4. Oligonucleotides used in this study

Name	Sequence
N405A_Fw	CATGGGATGGAAAACAGCCAAATATGGCACACTATATAAATC
N405A_Rev	TAGTGTGCCATATTTGGCTGTTTTCCATCCCATGGTATATC
N405A_Fw_Lss	TACAGGTTGGAAAACAGCCAAATATGGCACACTATATAAATC
N405A_Rev_Lss	AGTGTGCCATATTTGGCTGTTTTCCAACCTGTATTCGGCGTTG
T409V_Fw	ACAAACAAATATGGCGTGCTATATAAATCAGAGTCAG
T409V_Rev	CTCTGATTTATATAGCACGCCATATTTGTTTGTTTTC
Y411S_Fw	AAATATGGCACACTATCAAAATCAGAGTCAGCTAGCTTC
Y411S_Rev	AGCTGACTCTGATTTTGATAGTGTGCCATATTTGTTTG
F418V_Fw	CAGAGTCAGCTAGCGTCACACCTAATACAGATATAATAAC
F418V_Rev	ATCTGTATTAGGTGTGACGCTAGCTGACTCTGATTTATATAGTG
N421L_Fw	GCTAGCTTCACACCTCTTACAGATATAATAACAAGAACGAC
N421L_Rev	GTTATTATATCTGTAAGAGGTGTGAAGCTAGCTGACTC
I425A_Fw	ACCTAATACAGATATAGCAACAAGAACGACTGGTCCATTTAG
I425A_Rev	CCAGTCGTTCTTGTTGCTATATCTGTATTAGGTGTGAAGCTAG
T429V_Fw	ATAATAACAAGAACGGTTGGTCCATTTAGAAGCATG
T429V_Rev	CTTCTAAATGGACCAACCGTTCTTGTTATTATATCTG
D450N_Fw	CAAACAATTCATTATAATGAAGTGATGAAACAAGAC
D450N_Rev	GTTTCATCACTTCATTATAATGAATTGTTTGACCTG
E451M_Fw	ACAATTCATTATGATATGGTGATGAAACAAGACGGTCATG
E451M_Rev	GTCTTGTTTCATCACCATATCATAATGAATTGTTTGAC
V452A_Fw	TTCATTATGATGAAGCGATGAAACAAGACGGTCATG
V452A_Rev	ACCGTCTTGTTTCATCGCTTCATCATAATGAATTGTTTG
M453A_Fw	CATTATGATGAAGTGGCAAAACAAGACGGTCATGTTTG
M453A_Rev	ATGACCGTCTTGTTTTGCCACTTCATCATAATGAATTG
M461A_Fw	ACGGTCATGTTTGGGCAGGTTATACAGGTAACAGTG
M461A_Rev	TTACCTGTATAACCTGCCCAAACATGACCGTCTTGTTTC
Y472S_Fw	AGTGGCCAACGTATTTCCTTGCCTGTAAGAACATGGAAT
Y472S_Rev	TGTTCTTACAGGCAAGGAAATACGTTGGCCACTGTTAC
L473A_Fw	GGCCAACGTATTTACGCGCCTGTAAGAACATGGAATAAATC
L473A_Rev	CATGTTCTTACAGGCGCGTAAATACGTTGGCCACTGTTAC
W489L_Fw	ACTTTAGGTGTTCTTCTGGGAACTATAAAGGGATCCGGAG
W489L_Rev	TCCCTTTATAGTTCCCAGAAGAACACCTAAAGTATTAGTAG
W489L_Fw_Lss	TACTTTAGGTGTTCTTCTGGGAACTATAAAGCTCGAGCAC
W489L_Rev_Lss	GAGCTTTATAGTTCCCAGAAGAACACCTAAAGTATTAGTAG

Table 5. Data collection and refinement statistics

	Home source set	Synchrotron set
Data collection		
Space group	$P4_12_12$	$P4_12_12$
Cell dimensions		
a, *b*, *c* (Å)	47.2, 47.2, 123.1	47.1, 47.1, 122.4
α, β, γ (°)	90, 90, 90	90, 90, 90
Resolution (Å)	2.5(2.6-2.5)*	1.43 (1.47-1.43)
R_{merge}	12.8(21.5)	5.9 (341.3)
$I / \sigma I$	14.3(6.0)	21.6(1.1)
Completeness (%)	99.6(98.7)	98.9(98.4)
Redundancy	11.9(8.9)	24.3(24.7)
Refinement		
Resolution (Å)	2.5	1.43
No. reflections	5270	26342
R_{work} / R_{free}	25.4/29.0	19.9/23.0
No. atoms		
Protein	741	741
Ligand/ion	49	52
Water	3	24
B-factors		
Protein	27.7	43.4
Ligand/ion	29.7	44.2
Water	17.9	44.3
R.m.s. deviations		
Bond lengths (Å)	0.003	0.008
Bond angles (°)	1.18	1.49

A single crystal was used for both data collections.
*Values in parentheses are for highest-resolution shell.

Ligand		Source
	GMGM	Synthetic compound
	G5	Synthetic compound
	P4	Synthetic compound
	P4-G5	Synthetic compound
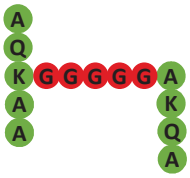	P5-G5-P4	Synthetic compound
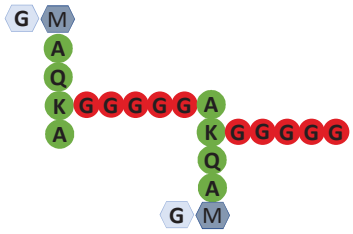	GM-P5-G5-GM-P4-G5	Peptidoglycan digestion (mutanolysin)

Supplementary Fig 1. *S. aureus* PG fragments used as SH3b ligands. The structure of each ligand, its name and method of preparation are indicated.

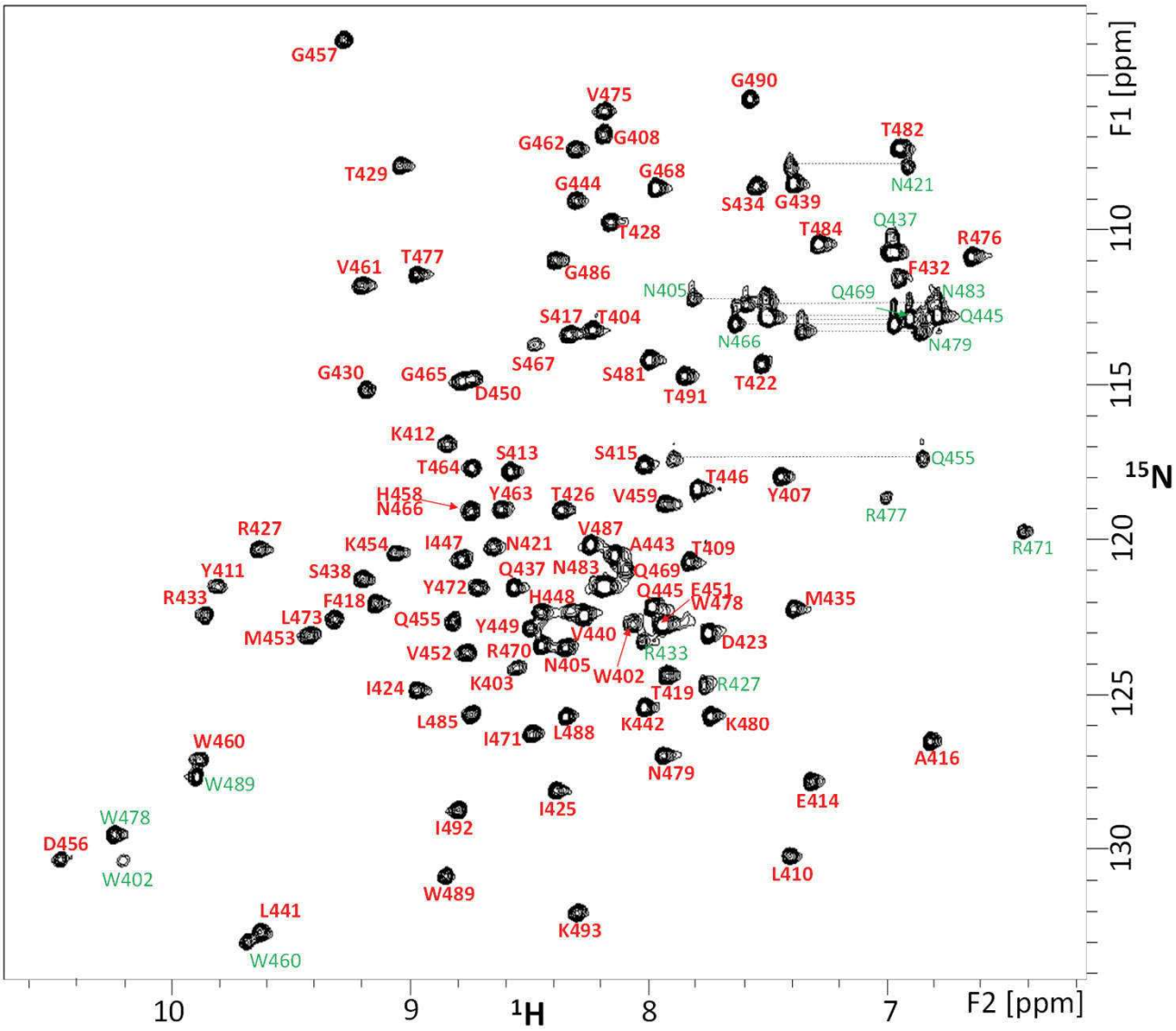

Supplementary Fig 2. Fully assigned ^{1}H- ^{15}N HSQC spectrum of the lysostaphin SH3b apo domain (residues 402-493). Assigned backbone amide resonances are shown. Side-chain resonances of tryptophan, glutamine and asparagine residues are indicated in green.

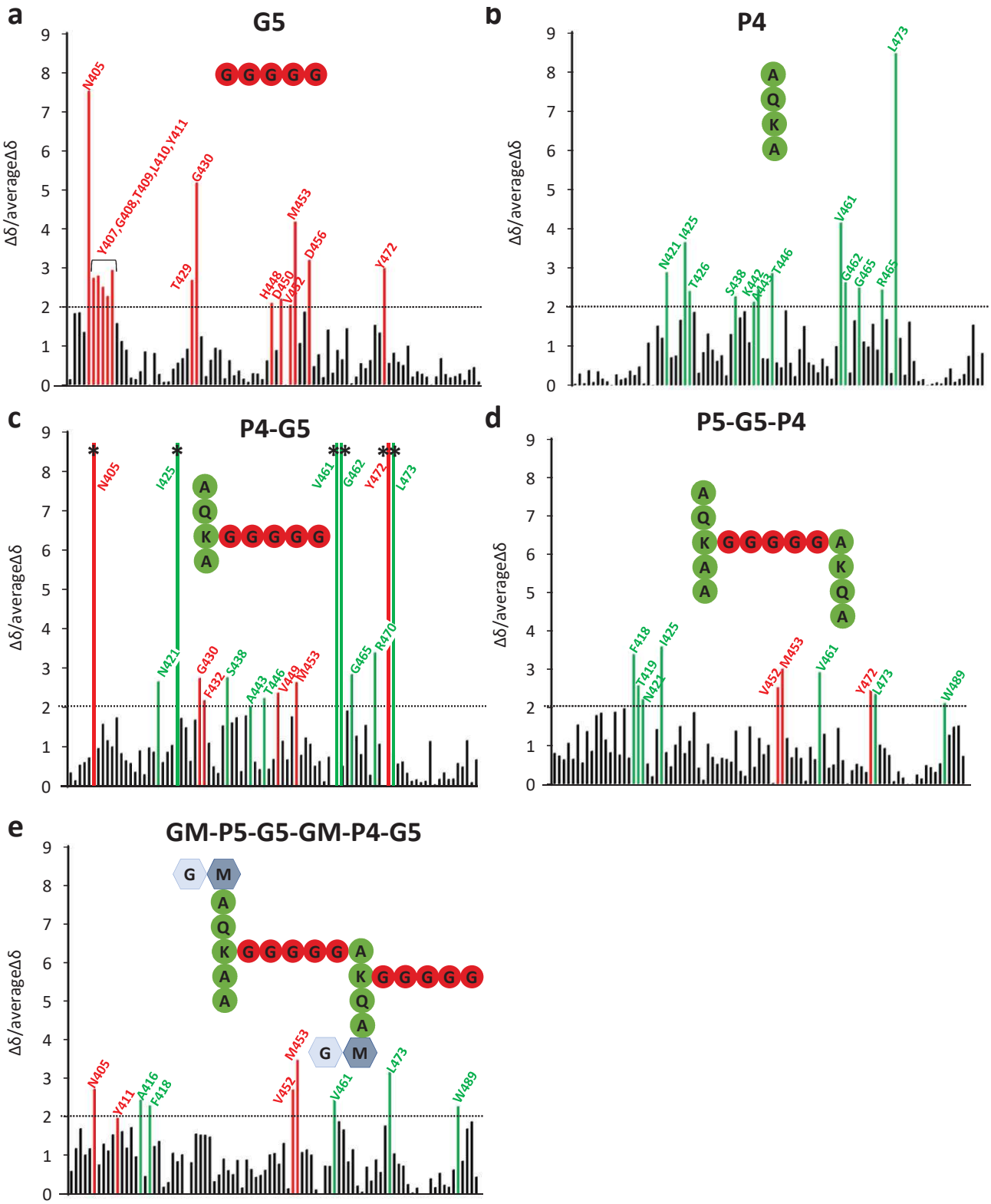

Supplementary Figure 3. Chemical shift perturbation (CSP) analysis of the SH3b protein interactions with a set of six different PG fragments derived from *S. aureus*. Histograms of the observed CSP values calculated as $\Delta\delta=(\Delta\delta H^2+(0.154x\Delta\delta N)^2)$, as a function of the amino acid sequence are shown. The *y*-axis represents the ratio between individual CSPs and the average CSP (taking all residues into account). An arbitrary threshold of 2 was chosen. Residues associated with CSPs above the threshold using G5 as a ligand are in red, those with CSPs above the threshold using P4 as a ligand are in green. Titrations were carried out using 50 µM of protein and G5 (**a**), P4 (**b**), P4-G5 (**c**), P5-G5-P4 (**e**) and GM-P5-G5-GM-P4-G5 (**f**). 0, 0.33, 0.66, 1, 2, 4, 8, 16, 32, and 64 equivalents of ligand were used in (**a**)-(**c**); 16 equivalents in (**d**), and only 4 equivalents in (**e**) as protein aggregation occurred.

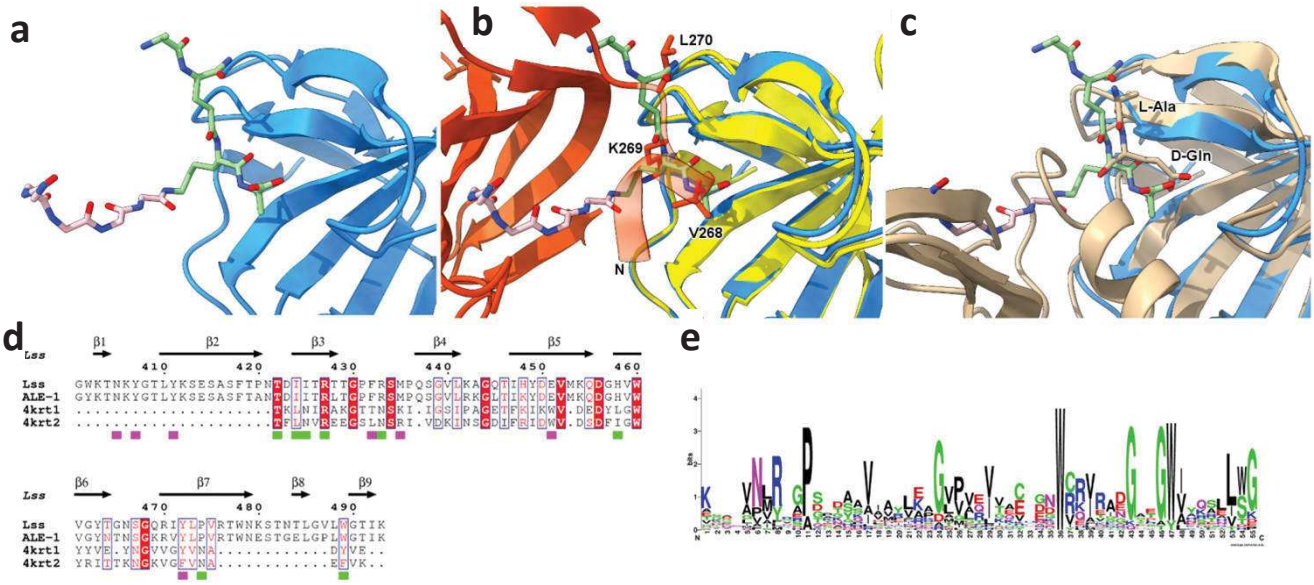

Supplementary Fig 4. Comparison of ligand-binding pocket to other SH3b structures and SH3 superfamily members. **a**, Lysostaphin SH3b domain in complex with the P4-G5 ligand. **b**, Superimposition of the structure shown in A onto the ALE-1 structure (1r77, two symmetry-related monomers orange and yellow). The P4-G5 ligand occupies the same space as an affinity purification tag (helical turn, N-terminus labelled). **c**, Superimposition of the structure shown in A onto the phi7917 structure (5D76, tan). Ligand P3(K)-P4(A) are sterically equivalent to tag residues K269 and V268, respectively. The phi7917 ligand (L-Ala-D-Gln) is positioned with its peptide bond over the P3-P4 peptide. **d,** Sequence alignment of Lysostaphin SH3b (SH3_5 subfamily) with ALE-1 (SH3_5) and the two tandem domains of *Clostridium* phage phiSM101 (4krt, SH3_3 subfamily), G5 and P4-ligating residues annotated with magenta and green block below text, respectively.

e, Weblogo (Crooks *et al.*, 2004) plot of sequence consensus of SH3_4 subfamily, identifying features with likely equivalence to SH3_3 and SH3_5 alignment: NxR (position 6-8, match lss I425-R427), W (36, match to W460), GxxGW (43-47, match to G468-Y472) and LWG (53-55, match to L488-G490). No structures are currently available for SH3_4 proteins, but structural comparison between Lss/ALE-1 and 4krt confirms conservation of the P-stem D-Ala(4)-carboxylate pocket.

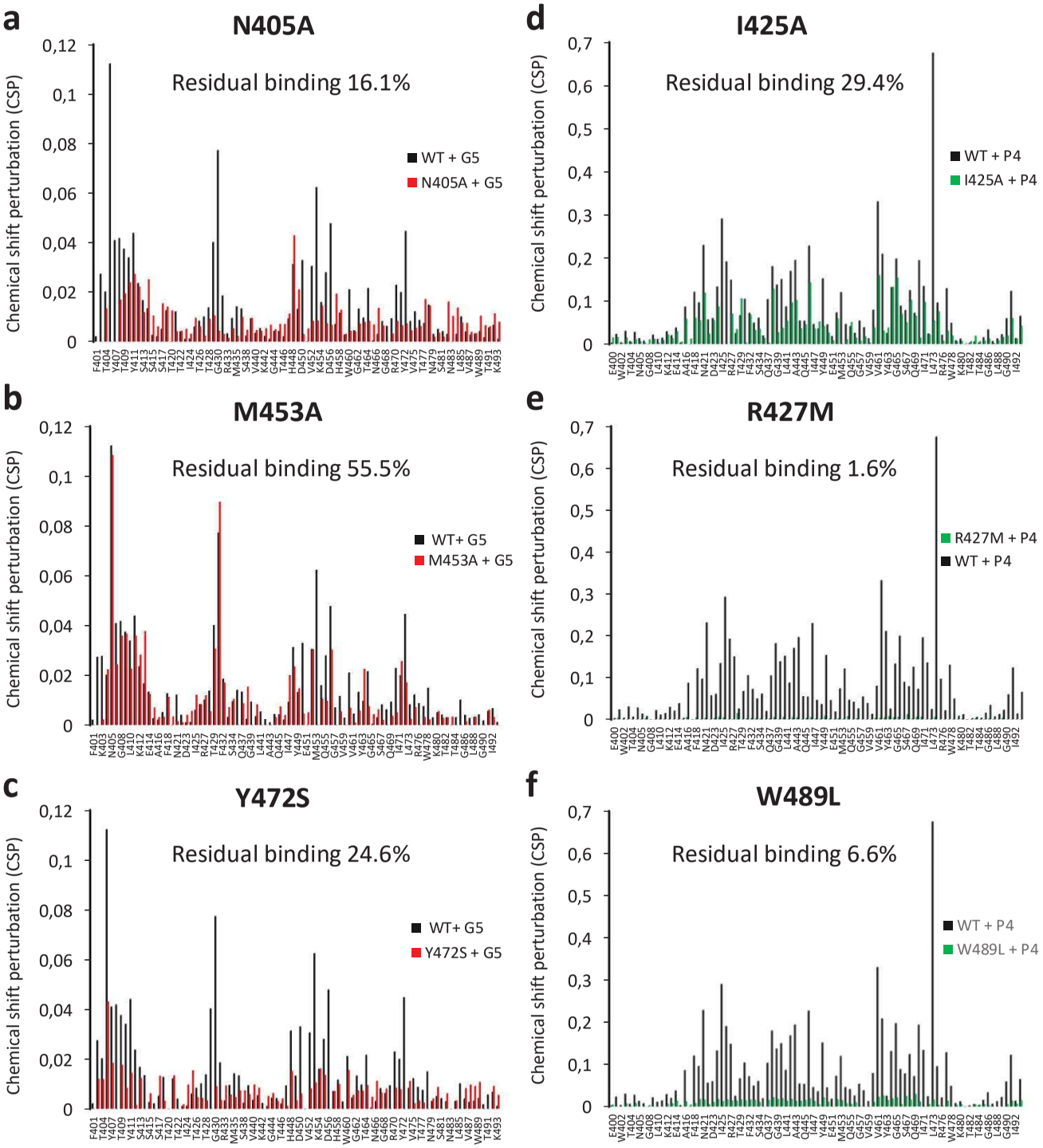

Supplementary Fig 5. Comparison of chemical shift perturbations (CSP) in wild-type and SH3b mutant domains associated with the binding to G5 and P4 ligands. Histograms show individual CSP values from the ^{15}N-HSQC titrations of N405A (**a**), M453A (**b**), and Y472S mutants (**c**) in red compared to the CSP values from the WT protein (in grey) following addition of 32 equivalents of G5. (**c**), (**d**) and (**e**) show CSPs from titrations of I425A, R427M and W489L, respectively (in green) compared to CSP values from the WT protein (in grey) following addition of 32 equivalents of P4. The percentage of residual binding activity deduced from the average CSP values is indicated.

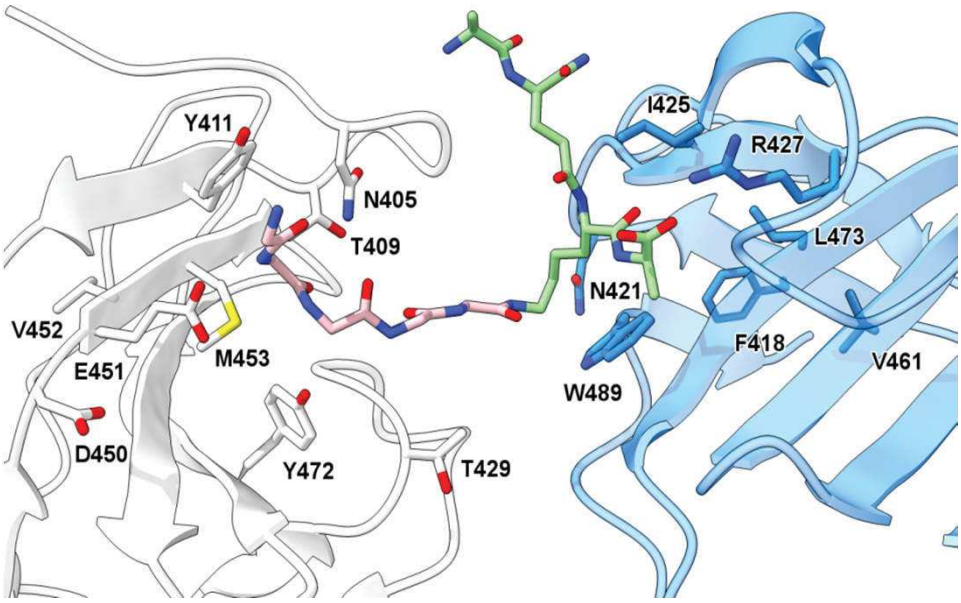

Supplementary Fig 6. Mutagenized residues at the SH3b:P4-G5 interaction interface. The representation is identical to figure 2, but displaying all residues selected for mutation in stick form (to avoid confusion, residues are only displayed once, from the SH3b domain that places them closest to the ligand).

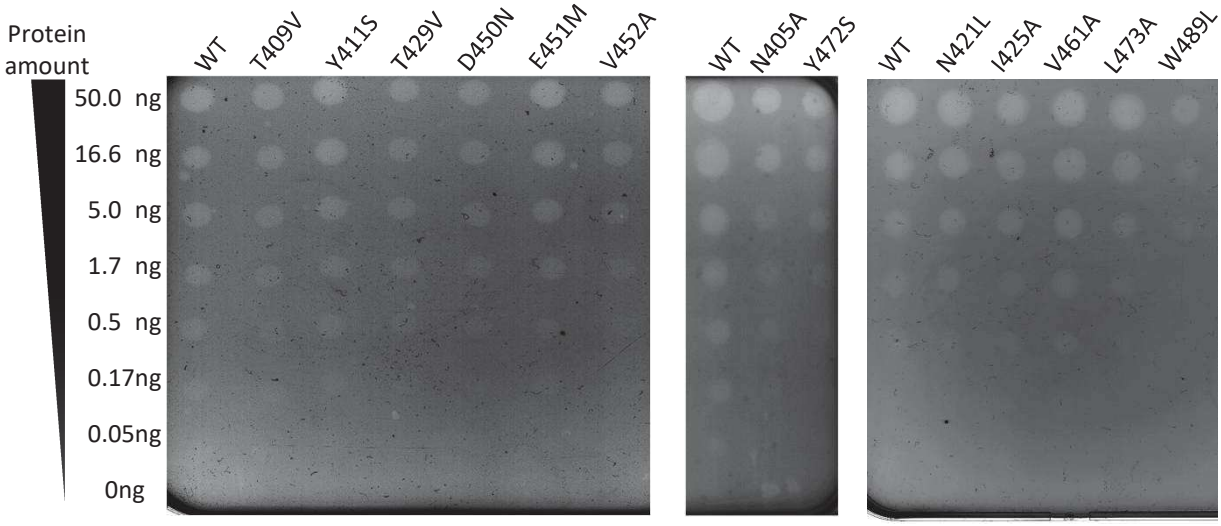

Supplementary Fig 7. Comparison of the enzymatic activity of lysostaphin (Lss) recombinant proteins containing mutations in the SH3b domain. Three independent series of purifications were carried out (left, middle and right panels), each including a wild-type protein as a control. Five µl corresponding to serial dilutions of recombinant Lss proteins were spotted on agar plates containing autoclaved *S. aureus* cells (final OD_{600} of 1) as a substrate. Lytic activities were detected as clearing zones and compared by determining the lowest amount of enzyme giving a detectable digestion of the substrate.

N-terminally His-tagged SH3b (pET-SH3b) for NMR analyses; residues 402-493

MGHHHHHHEFWKTNKYGTLYKSESASFTPNTDIITRTTGPFRSMPQSGVLKAGQTIHYDEVMKQDG
HVWVGYTGNSGQRIYLPVRTWNKSTNTLGVLWGTIK

N-terminally His-tagged SH3b (pET-SH3b-TEV) for X-ray crystallography; residues 402-493

MSGHHHHHHAMGENLYFQG↓SWKTNKYGTLYKSESASFTPNTDIITRTTGPFRSMPQSGVLKAGQTIH
YDEVMKQDGHVWVGYTGNSGQRIYLPVRTWNKSTNTLGVLWGTIKVLWGTIK

C-terminally his-tagged SH3b-mNeonGreen fusion (pET-SH3b-NG) for binding assays; residues 401-493

MGWKTNKYGTLYKSESASFTPNTDIITRTTGPFRSMPQSGVLKAGQTIHYDEVMKQDGHVWVGYTG
NSGQRIYLPVRTWNKSTNTLGVLWGTIKGSGGSGSGGSNNSGMVSKGEEDNMASLPATHELHIFGSI
NGVDFDMVGQGTGNPNDGYEELNLKSTKGDLQFSPWILVPHIGYGFHQYLPYPDGMSPFQAAMVD
GSGYQVHRTMQFEDGASLTVNYRYTYEGSHIKGEAQVKGTGFPADGPVMTNSLTAADWCRSKKTYPN
DKTIISTFKWSYTTGNGKRYRSTARTTYTFAKPMAANYLKNQPMYVFRKTELKHSKTELNFKEWQKAFT
DVMGMDELYKHHHHHH

Full length lysostaphin (pET-Lss) for activity assays; residues 248-493

MAATHEHSAQWLNNYKKGYGYGPYPLGINGGMHYGVDFFMNIGTPVKAISSGKIVEAGWSNYGGG
NQIGLIENDGVHRQWYMHLSKYNVKVGDYVKAGQIIGWSGSTGYSTAPHLHFQRMVNSFSNSTAQD
PMPFLKSAGYGKAGGTVTPTPNTGWKTNKYGTLYKSESASFTPNTDIITRTTGPFRSMPQSGVLKAGQ
TIHYDEVMKQDGHVWVGYTGNSGQRIYLPVRTWNKSTNTLGVLWGTIKLEHHHHHH

Supplementary Fig 8. Amino acid sequences of the recombinant wild-type proteins used in this study. In each case, both the plasmid encoding the recombinant SH3b protein (in brackets) and the experiment it was used for are indicated. The SH3b domain is in red, amino acids encoded by the expression vector in grey, linker in blue and mNeonGreen in green. The TEV cleavage site is indicated by an arrow.

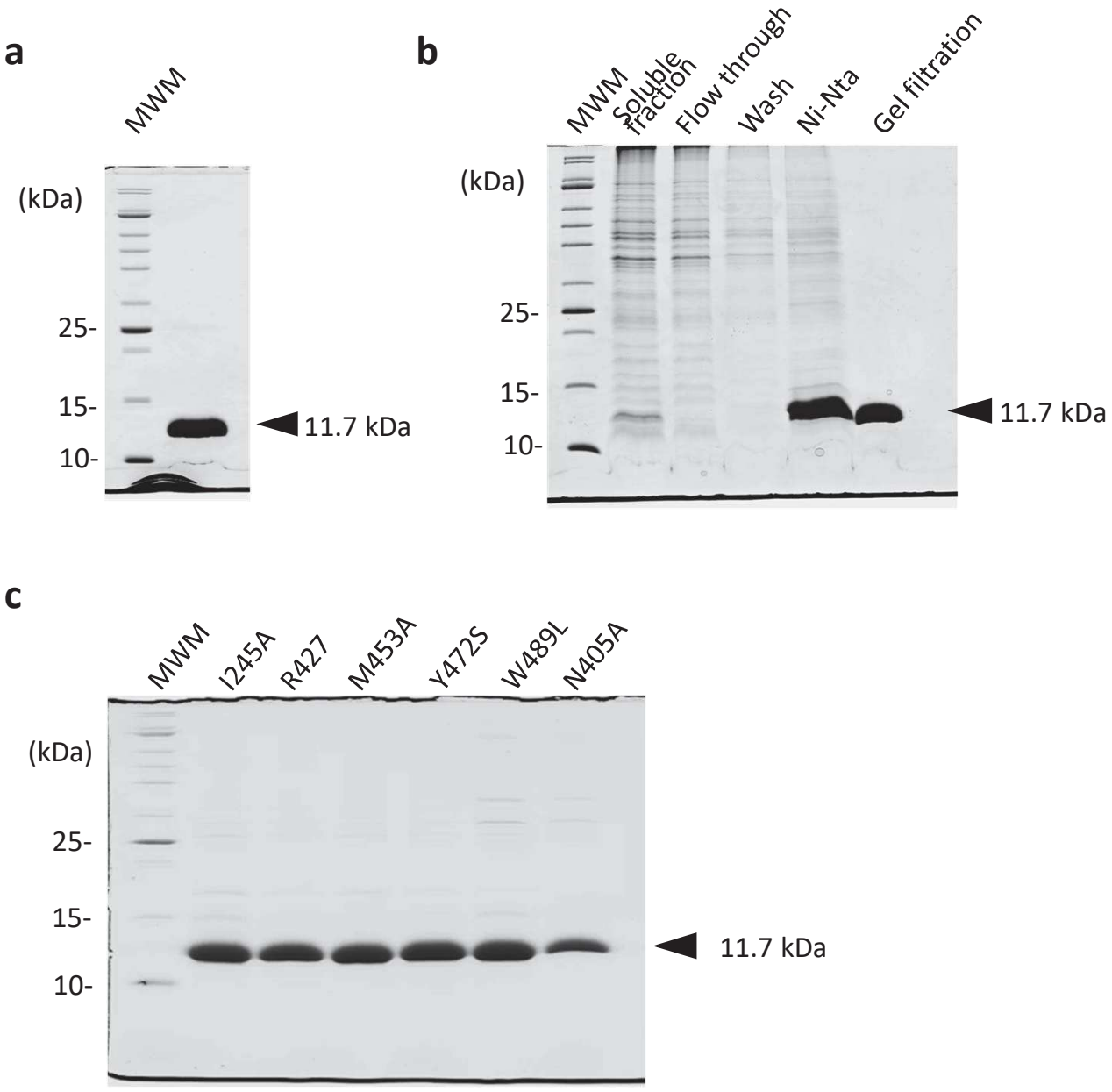

Supplementary Fig 9. SDS-PAGE analysis of recombinant proteins used for NMR studies. **a,** doubly labelled SH3b domain for spectrum assignment described in Supplementary Fig. 2. **b**, singly labelled His-tagged SH3b domain used for NMR titrations with ligands described in Fig. 1 and Supplementary Fig. S3. **c**, singly labelled His-tagged derivatives used for the mutational analysis of the SH3b domain described in Supplementary Fig. 5.

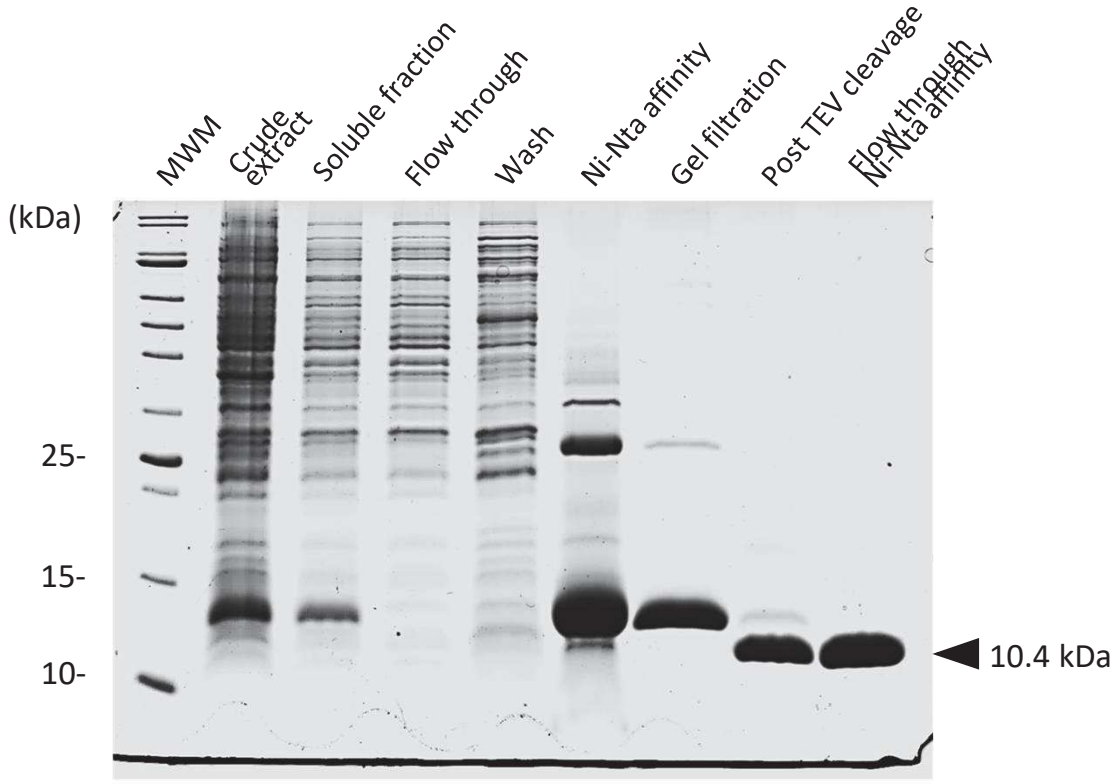

Supplementary Fig 10. SDS-PAGE analysis of recombinant proteins used for X-ray crystallography. The different steps of the purification are described. The final purification product corresponding to the SH3b domain without any His-tag was used for co-crystallisation experiments.

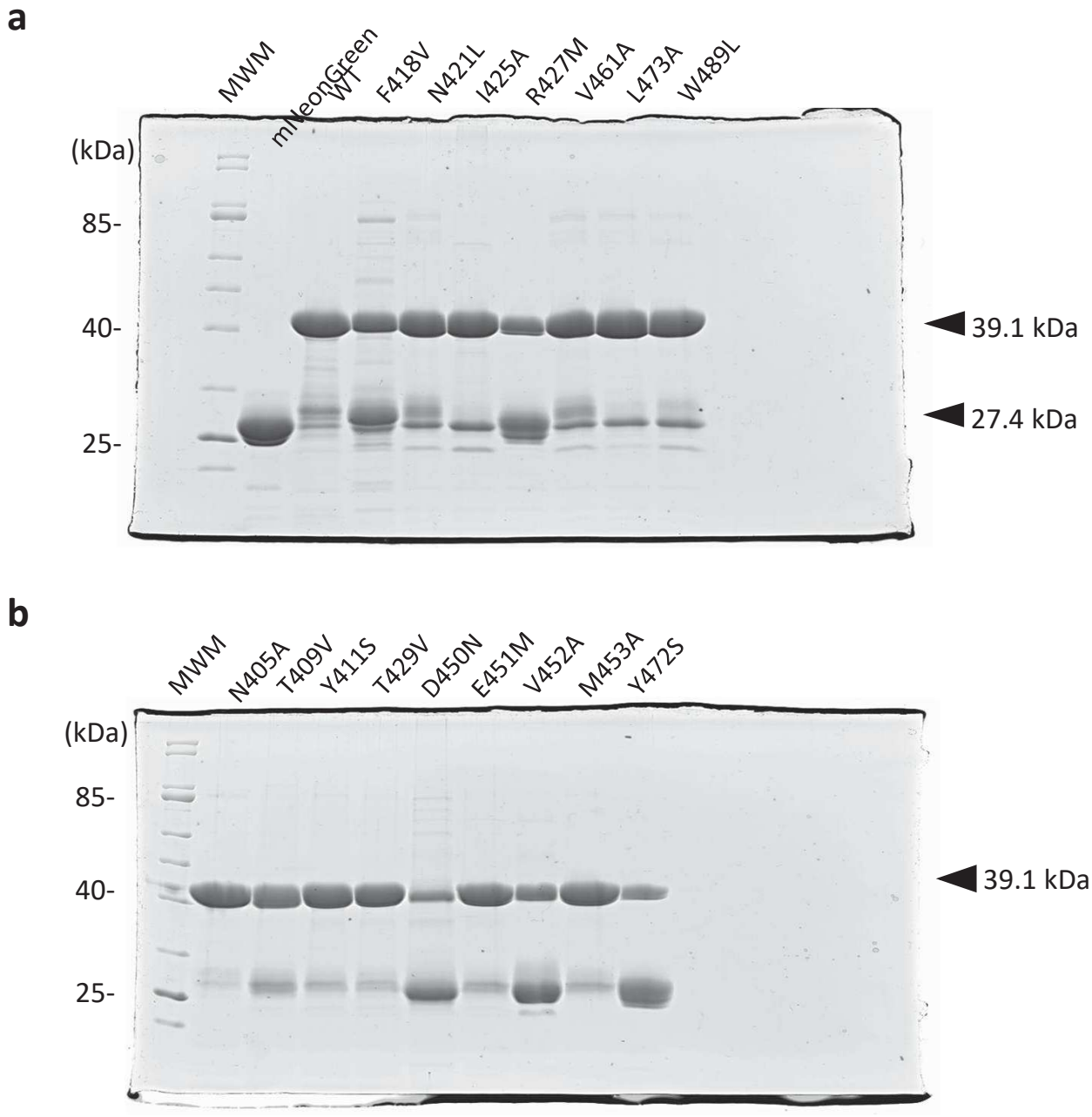

Supplementary Fig 11. SDS-PAGE analysis of recombinant SH3bp-mNeonGreen fusion proteins used for PG binding assays. a, mNeonGreen control and SH3b mutants harbouring mutations in the residues involved in the interaction with G5 ligands. **b**, SH3b mutants harbouring mutations in the residues involved in the interaction with P4 ligands. The amount of protein per binding assay was adjusted using the fluorescent signal intensity of the full-length protein.

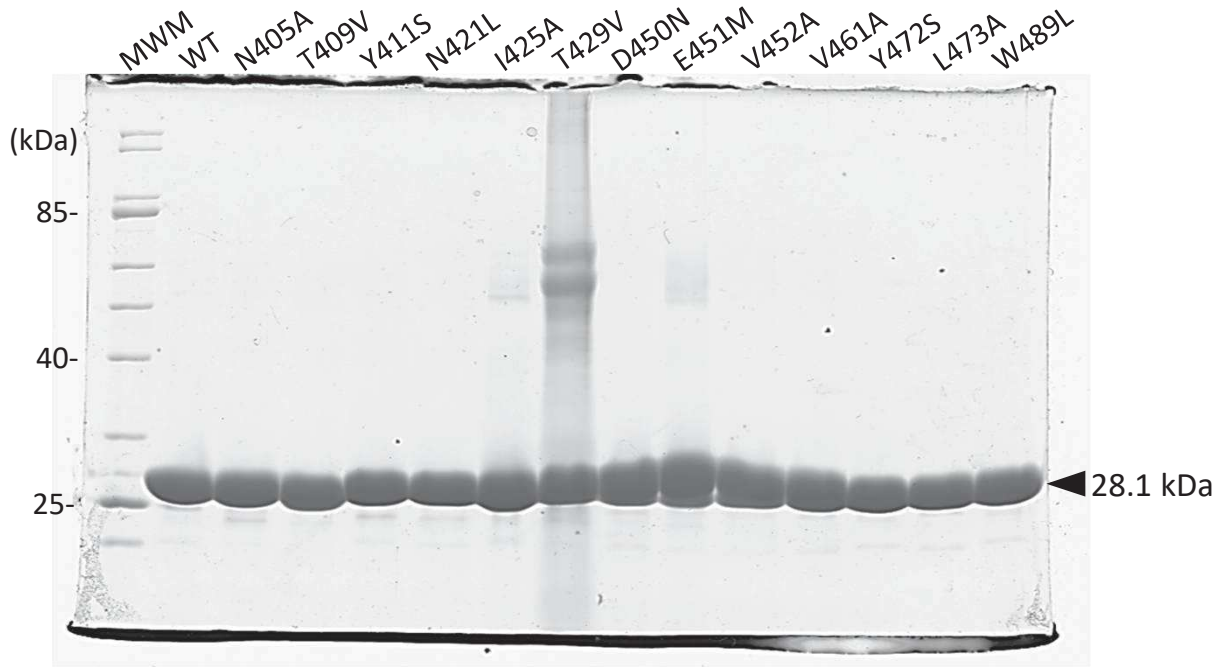

Supplementary Fig 12. SDS-PAGE analysis of recombinant SH3bp-mNeonGreen fusion proteins used for PG binding assays. a, mNeonGreen control and SH3b mutants harbouring mutations in the residues involved in the interaction with G5 ligands. **b**, SH3b mutants harbouring mutations in the residues involved in the interaction with P4 ligands. The amount of protein per binding assay was adjusted using the fluorescent signal intensity of the full-length protein.